

A FUSE Survey of Molecular Hydrogen in Intermediate-Velocity Clouds in the Milky Way Halo

Philipp Richter^{1,2}, Bart P. Wakker¹, Blair D. Savage¹
and

Kenneth R. Sembach³

ABSTRACT

Far Ultraviolet Spectroscopic Explorer (FUSE) data is used to investigate the molecular hydrogen (H_2) content of intermediate-velocity clouds (IVCs) in the lower halo of the Milky Way. We analyze interstellar absorption towards 56 (mostly extragalactic) background sources to study H_2 absorption in the Lyman- and Werner bands in 61 IVC components at H I column densities $\geq 10^{19} \text{ cm}^{-2}$. For data with good S/N (~ 9 per resolution element and higher), H_2 in IVC gas is convincingly detected in 14 cases at column densities varying between $\sim 10^{14}$ and $\sim 10^{17} \text{ cm}^{-2}$. We find an additional 17 possible H_2 detections in IVCs in FUSE spectra with lower S/N. The molecular hydrogen fractions, f , vary between 10^{-6} and 10^{-3} , implying a dense, mostly neutral gas phase that is probably related to the Cold Neutral Medium (CNM) in these clouds. If the H_2 stays in formation-dissociation equilibrium, the CNM in these clouds can be characterized by compact ($D \sim 0.1 \text{ pc}$) filaments with volume densities on the order of $n_H \sim 30 \text{ cm}^{-3}$. The relatively high detection rate of H_2 in IVC gas implies that the CNM in these clouds is ubiquitous. More dense regions with much higher molecular fractions may exist, but it would be difficult to detect them in absorption because of their small size.

Subject headings: ISM: clouds – ISM: abundances – quasars: absorption lines – Galaxy: halo

1. Introduction

Direct observational information on the most abundant interstellar molecule in the Universe, molecular hydrogen (H_2), is difficult to obtain. In diffuse interstellar gas, H_2 can be studied directly by way of far-ultraviolet (FUV) absorption spectroscopy in its electronic Lyman and Werner bands in the wavelength regime between 912 and 1130 Å toward UV-bright background sources, such as early type stars, supernovae, quasars (QSOs) and active galactic nuclei (AGNs). In the low-

redshift Universe, this bandpass is accessible only with space-based instrumentation. Previous FUV satellites, such as *Copernicus* and ORFEUS, observed only very nearby stars and a few selected distant objects. An overall assessment of the H_2 content of the diffuse ISM outside the Milky Way disk and the Magellanic Clouds was not possible before 1999, when the *Far Ultraviolet Spectroscopic Explorer* (FUSE) was launched. The high sensitivity of FUSE allows observations of H_2 absorption in regions outside the Milky Way disk towards a large number of extragalactic background sources. Such observations reveal the abundance and properties of diffuse molecular gas in a variety of different environments.

Particularly promising regions for studies of H_2 are the Milky Way halo and its neutral gas clouds that move with intermediate ($30 \leq |v_{\text{LSR}}| \leq 90$

¹Department of Astronomy University of Wisconsin-Madison, 475 N. Charter Street, Madison, WI 53706; richter@astro.wisc.edu

²Osservatorio Astrofisico di Arcetri, Largo E. Fermi 5, 50125 Florence, Italy

³Space Telescope Science Institute, 3700 San Martin Drive, Baltimore MD 21218

km s^{-1} ; IVCs) and high ($|v_{\text{LSR}}| \geq 90 \text{ km s}^{-1}$; HVCs) radial velocities several kiloparsecs above the Galactic plane. Recent studies with FUSE and the *Space Telescope Imaging Spectrograph* (STIS) have shown that the chemical composition of these clouds is not uniform, with metallicities varying between ~ 0.1 and ~ 1.0 solar (Wakker et al. 1999; Richter et al. 2001a, 2001b; Lu et al. 1998; Gibson et al. 2000, 2001; Wakker 2001). The results imply a separation into three different groups of Galactic halo clouds: (1) Gas that has been ejected out of the Milky Way disk by a “Galactic Fountain” (Shapiro & Field 1976) or similar processes, having ~ 1.0 solar abundances. All of the IVCs probably fall into this category. (2) Gas that has been brought into the Milky Way halo due to tidal interactions with the Magellanic Clouds, having metallicities similar to that of the Magellanic Clouds (~ 0.3 solar for the Magellanic Stream). (3) Low-metallicity gas (~ 0.1 solar abundances) that is infalling into the Galactic halo from intergalactic space (e.g., HVC Complex C). Because of the varying metal and dust content of IVCs and HVCs, and the reduced UV radiation field above the Galactic plane, IVCs and HVCs may serve as important interstellar laboratories to study H_2 formation- and dissociation processes under conditions that are also found in more distant regions of the Universe (e.g., in intergalactic Ly α absorbers) for which detailed H_2 absorption spectroscopy is often impossible.

Except for some IVCs that are close to the disk (the Draco cloud - Mebold et al. 1985, and IV 21 - Weiss et al. 1999, Heithausen et al. 2001), no CO emission or absorption has been detected in Galactic halo clouds so far. H_2 was found for the first time in HVC gas (Richter et al. 1999) and IVC gas (Gringel et al. 2000) in data of the ORFEUS satellite, followed by further detections with FUSE (Sembach et al. 2001a; Richter et al. 2001a). In a previous paper (Richter et al. 2001c), we studied H_2 absorption in two prominent metal-poor HVCs, the Magellanic Stream and Complex C. While H_2 is clearly detected in the Magellanic Stream (see also Sembach et al. 2001a), there is no evidence for the presence of H_2 in the metal- and dust-poor Complex C (Richter et al. 2001b). This implies that the formation and maintainance of diffuse H_2 in halo clouds is tightly correlated to the availability of interstellar dust grains, on whose surface the

H_2 formation proceeds most efficiently (see, e.g., Shull & Beckwith 1982).

In this paper we investigate the distribution of H_2 in IVCs toward 56 background sources. The data sample nearly all of the most prominent, large IVCs located predominantly in the northern Galactic sky. These IVCs are: the Intermediate-Velocity Arch (IV Arch), the Low-Latitude Intermediate-Velocity Arch (LLIV Arch), and the Intermediate-Velocity Spur (IV Spur) in the northern Galactic sky, and Complex gp and the Pegasus-Pisces Arch (PP Arch) in the southern sky. As summarized by Wakker (2001), all of these IVCs are known to have roughly solar, or slightly sub-solar metallicities, and are located between 0.3 and 2.1 kpc away from the Galactic plane; thus they are in the “lower” Galactic halo. Distance brackets for IVCs are derived by comparing IVC absorption line detections and non-detections toward stars at known distances and z -heights (see Wakker 2001 for details).

In Figure 1 we show the negative velocity $\text{H}\alpha$ IVC sky based on 21cm data from the Leiden-Dwingeloo Survey (LDS; Hartmann & Burton 1997) at $\text{H}\alpha$ column densities $N(\text{H}\alpha) \geq 2 \times 10^{19} \text{ cm}^{-2}$. The various IVC complexes are identified and explained in detail by Wakker (2001). Intermediate-velocity $\text{H}\alpha$ above this column density covers a significant portion of the sky (~ 35 percent for $30 \leq |v_{\text{LSR}}| \leq 90 \text{ km s}^{-1}$), but it is very likely that the sky-coverage is much higher for low-column density $\text{H}\alpha$ gas below the detection limit of the 21cm observations. The high sky coverage of IVC gas in the halo or disk-halo interface underlines the importance of the IVC phenomenon to an understanding of the ISM of the Milky Way, although there do not exist many systematic studies of IVCs in the literature. As pointed out by Kulkarni & Fich (1985), IVCs actually contain much of the kinetic energy of the total Galactic ISM. Moreover, IVCs appear to have a mass circulation rate much higher than the HVCs, and high enough to produce the O VI seen in the thick Galactic disk, if the IVCs represent the return flow of a Galactic Fountain (see Savage et al. 2002).

Some of the IVCs have been studied in detail using FUSE absorption line data (LLIV Arch, Richter et al. 2001a; IV Arch, Richter et al. 2001b). The elemental depletion pattern observed in IVCs implies that these clouds contain dust grains, but

the surface properties of these grains, important for the H₂ formation, are unknown. With respect to their velocities, abundances, and distances, it appears likely that IVCs represent the cooled return flow of a Galactic Fountain (Shapiro & Field 1976). One of our sight lines (Mrk 876) samples the Draco cloud ($z = 0.3 - 0.8$ kpc), one of the two IVCs at lower z that is known to contain CO. It is not yet clear whether the Draco cloud falls into the same class of objects as the other IVCs cited above (possibly, as a final stage of the Galactic Fountain process), or whether it represents a Galactic molecular cloud at unusually high Galactic latitudes and z -height. Our FUSE data also sample a variety of other small IVCs in the northern and southern Galactic sky. Distances and metallicities for these IVCs are unknown, but we have formally included these clouds in our sample, based on criteria that are described in §4.

This paper is organized as follows: In §2 we discuss the FUSE observations and the data handling. In §3 we analyze in detail molecular hydrogen absorption in the IV Arch in the FUSE spectrum of the quasar PG 1351+640. In §4 we present a survey of H₂ in IVCs toward 56 (mostly extragalactic) background sources. A comparison between the H₂ and the H I sky at intermediate velocities is given in §5. In §6 and §7 we investigate the origin and physical conditions of the diffuse molecular gas in the lower halo. A discussion of our observations is presented in §8. We summarize our study in §9.

2. Observations and Data Handling

In this paper we are making use of FUSE absorption line data of ~ 200 sources, predominantly extragalactic objects (QSOs, Seyferts, Galaxies, BLLacs), as well as two distant ($d > 5$ kpc) Galactic halo stars. This data is available from the FUSE survey of interstellar O VI in the thick disk of the Milky Way and in high-velocity clouds (Wakker et al. 2002; Savage et al. 2002; Sembach et al. 2002). A detailed description of the FUSE data and the analysis method is provided by Wakker et al. (2002). We briefly summarize the observations and the data reduction process. The FUSE spectra were collected in the time between November 1999 and December 2001 as part of various Principal-Investigator (PI) projects and

Guest-Investigator (GI) projects.⁴ FUSE is equipped with four co-aligned prime-focus telescopes, Rowland-type spectrographs, and two microchannel plate detectors, in total covering the wavelength range from 905 to 1187 Å. Four independent channels are available, two having a Al+LiF coatings (for $\lambda \geq 1000$ Å) and two having SiC surfaces ($\lambda \leq 1100$ Å). There are three entrance apertures, LWRS ($30''.0 \times 30''.0$), MDRS ($4''.0 \times 20''.0$), and HIRS ($1''.25 \times 20''.0$). Details about the instrument and its in-orbit performance can be found in Moos et al. (2000) and Sahnow et al. (2000).

Most of the data that is used here were recorded through the large aperture (LWRS) and in the photon-address mode, in which the X/Y location, the arrival time, and the pulse height of each detection are stored in a photon list. All spectra have been reduced using the CALFUSE standard pipeline (v1.8.7) that corrects for detector backgrounds, spacecraft orbital motions, and geometrical distortions (Sahnow et al. 2000). A wavelength calibration was made for each individual spectrum by adjusting various atomic lines (e.g., Si II $\lambda 1020.7$, Ar I $\lambda 1048.2$) and molecular hydrogen lines to match the distribution of H I emission along each sight line (see Wakker et al. 2002) on the LSR velocity scale. We estimate an accuracy of $\sim 10 - 15$ km s⁻¹ for the velocity calibration. The spectral resolution of the FUSE data is ~ 20 km s⁻¹, with slight variations ($\sim \pm 5$ km s⁻¹) within the data set. The fluxes of our background sources vary between 0.1 and 60×10^{-14} erg cm⁻² s⁻¹ Å⁻¹ (see Wakker et al. 2002). Only a fraction of the entire data set (~ 50 percent) can actually be used to study interstellar absorption in the halo at a sufficient continuum flux. The data for each sight line were rebinned in an appropriate manner in order to improve the signal-to-noise ratio (S/N). For the spectra that are actually used to study IVC H₂ absorption in this study (56 spectra), bin sizes range between 3 and 10 pixels, corresponding to ~ 6 to ~ 20 km s⁻¹. The S/N in the data varies between 3 and 30 (these values represent the S/N per resolution element; see also Wakker et al. 2002). Continua were fitted using low-order polynomials. Most of the continua are relatively

⁴All the FUSE data presented are publicly available at the MAST archive at <http://archive.stsci.edu/fuse>.

flat, reflecting the smooth nature of the UV spectrum of QSOs and other extragalactic background sources. In some cases, emission that is associated with the background object complicates the continuum placement, but the corresponding continuum variations arise on a scale that is much larger than that of the interstellar absorption lines. For these cases, the continuum was fitted locally in the vicinity of each line.⁵ Equivalent widths were measured by fitting multi-component Gaussian line profiles to the data. This method is particularly helpful to reproduce a multi-component absorption in a spectrum with low S/N and larger bin sizes. Equivalent width errors are based on photon statistics and continuum placement errors.

3. H₂ Absorption in the IV Arch toward PG 1351+640

In this section we present a detailed description and discussion of H₂ absorption in the Intermediate-Velocity Arch (IV Arch) in the FUSE spectrum of the quasar PG 1351+640, which represents the best example of molecular absorption in intermediate-velocity halo gas. For most of the other sight lines presented later, such a detailed study is not possible due to the lower data quality and the less pronounced nature of the H₂ absorption. This section, however, may serve as an introduction to the general analysis method that we will also use for the other sight lines discussed in §4.

Figure 2 presents the sight-line structure towards PG 1351+640, as seen in Effelsberg H I 21cm emission data (top panel, from Wakker et al. 2001) and in atomic absorption from P II $\lambda 1152.8$, Si II $\lambda 1020.7$, and Fe II $\lambda 1122.0$ (lower three panels) from FUSE data, plotted on a LSR radial velocity scale. The main emission and absorption components include: (1) local Milky Way gas near 0 km s^{-1} , (2) the IV Arch seen near -50 km s^{-1} , and (3) HVC Complex C at -155 km s^{-1} . Detailed maps of 21cm emission in the IV Arch and Complex C can be found in Kuntz & Danly (1996) and Wakker (2001). As the H I emission profile shows, all three major components have substructure, for instance a weak second IVC component near -74 km s^{-1} , which is also seen in atomic absorption.

⁵Similary, this method was used for the two stellar background sources that have more irregularly shaped continua.

The Effelsberg data yield H I column densities of $1.12 \times 10^{20} \text{ cm}^{-2}$ for the main IVC component at -50 km s^{-1} , and $1.58 \times 10^{18} \text{ cm}^{-2}$ for the weaker component at -74 km s^{-1} . The -50 km s^{-1} component is associated with the IV 19 core (see Kuntz & Danly 1996), while the -74 km s^{-1} component is part of core IV 9.

H₂ absorption in the IV Arch toward PG 1351+640 is found in 29 lines in rotational levels $J = 0$ to 3 at a radial velocity of $v_{\text{LSR}} \approx -50 \text{ km s}^{-1}$, representing the main IVC component along this sight line (see above)⁶. Figure 3 presents a portion of the FUSE spectrum of PG 1351+640 in the wavelength region of the H₂ Lyman 2 – 0 band, together with a two-component Gaussian fit of the data. Figure 4 shows a selection of velocity profiles for the rotational ground states $J = 0$ and 1. Similary, Figure 5 presents velocity profiles for the excited rotational levels $J = 2$ and 3. Clearly, H₂ absorption near -50 km s^{-1} is present at moderate strength in all of the lines shown, whereas H₂ absorption from the local Galactic disk gas is seen near 0 km s^{-1} . We have measured equivalent widths for the H₂ absorption in the IV Arch (Table 1) and have fitted the data to curves of growth for each individual rotational level, J , deriving logarithmic column densities, $\log N(J)$. For $J = 0$, the data fits best on a curve of growth with a very low Doppler parameter of $b = 2.3_{-0.5}^{+1.1} \text{ km s}^{-1}$ (Figure 6), implying that the H₂ gas in the rotational ground state resides in a very confined region in the IV Arch that has a very low velocity dispersion. For $J = 1, 2$ and 3, we find $b = 3.5_{-0.9}^{+1.4} \text{ km s}^{-1}$, possibly indicating that the excited molecular hydrogen gas is situated in a less confined region. The different b values may reflect a core-envelope structure of the H₂, in which the more turbulent gas in the outer parts is rotationally excited, whereas the inner, less turbulent part of the H₂ gas remains mostly in the rotational ground state. However, the interpretation of the $J = 0$ data points in Figure 6 is difficult, since the lower b value for the rotational ground state is determined mainly by the R(0) line with the lowest f -value (R(0),0-0 $\lambda 1108.128$; see Table 1). If the equivalent width of this line is overestimated by $1 - 2\sigma$ (e.g., due to a noise peak or an unidentified

⁶No H₂ absorption is evident in the weaker -74 km s^{-1} component; see also Table 2.

intergalactic absorption feature), the data points for $J = 0$ would also fit the curve of growth for the $J = 1 - 3$ lines with $b = 3.5 \text{ km s}^{-1}$, and the H_2 column density for $J = 0$ would be lower. This seems somewhat unrealistic though, because the $N(0)/N(1)$ ratio (already quite low with the two different b values) would further decrease, and the H_2 column density distribution for $J = 0$ and 1 could not be fitted by an excitation temperature that would be consistent with the relatively low value for $\log N(2)$ (see Figure 7). Thus, we adopt the two different b values for $J = 0$ and $J = 1 - 3$ in the following discussions, but note that more precise data are required to improve the determination of b for $J = 0$.

Individual column densities, $\log N(J)$, based on the two different b values for $J = 0$ and $J = 1 - 3$ given above, are listed in Table 1. The total H_2 column density, $\log N(\text{H}_2)$, is 16.43 ± 0.14 (1σ error), and the fraction of hydrogen in molecular form is $\log f = \log [2N(\text{H}_2)/(N(\text{H I}) + 2N(\text{H}_2))] = -3.3$, based on the H I 21cm data from Effelsberg. We have derived excitation temperatures for the H_2 gas by fitting the H_2 rotational level population to a theoretical Boltzmann distribution (Figure 7). We find an excitation temperature, T_{01} , of 141 ± 20 K for $J = 0$ and 1, possibly representing an upper limit for the kinetic temperature of the gas in the interior of the cloud. The temperature in the inner core of the cloud could be lower, if part of the H_2 gas with $J = 1$ resides in a more extended region than the $J = 0$ gas, as implied by the slightly higher b value for $J = 1$. For $J = 2, 3$ and 4 (upper limit) we find $T_{24} = 885 \pm 270$ K. This high excitation temperature probably reflects several competing processes, such as UV pumping and H_2 formation pumping (see Shull & Beckwith 1982). The column density ratios $N(3)/N(1)$, $N(4)/N(2)$, and $N(5)/N(3)$ can be used to disentangle the various excitation mechanisms to a certain degree (e.g., Browning, Tumlinson & Shull 2002), but such an interpretation is difficult if information on the higher rotational levels is limited. In view of the uncertainties for $N(2)$ and $N(3)$, and the fact that no H_2 is detected for $J = 4$ and 5 we therefore refrain from a more detailed analysis of the rotational excitation of the IVC H_2 gas toward PG 1351+640.

The total H_2 column density in the IV Arch towards PG 1351+640, $\log N = 16.43 \pm 0.14$, is the

highest that has been reported for intermediate-velocity clouds so far. This is not surprising, however, since the line of sight to PG 1351+640 passes through the IV Arch in a region with an H I column density of $\log N = 20.05$, which is substantially higher than in other directions for which H_2 absorption in IVCs was measured before (e.g., Gringel et al. 2000; Richter et al. 2001a, 2001b).

From a measurement of several atomic absorption lines of Fe II , Si II , and P II in the PG 1351+640 spectrum we find atomic column densities of $\log N(\text{Fe II}) \approx 15.1$, $\log N(\text{Si II}) \approx 15.2$, and $\log N(\text{P II}) \approx 13.6$ for the IV 19 component at -50 km s^{-1} . Together with the H I column density of $\log N = 20.05$ from the 21cm data we derive logarithmic gas-phase abundances, $[X/\text{H}] = \log(N_X/N_{\text{H I}}) - \log(X/\text{H})_{\odot}$, of $[\text{Fe}/\text{H}] \approx -0.4$, $[\text{Si}/\text{H}] \approx -0.4$, and $[\text{P}/\text{H}] \approx 0.0$ (the values for $\log(X/\text{H})_{\odot}$ are from Anders & Grevesse 1989; Grevesse & Noels 1993). Thus, the FUSE and the H I 21cm data imply that IV 19 has a nearly solar abundance (as sampled by P), similar to what is found for the IV Arch in the direction of PG 1259+593 (Richter et al. 2001b). Fe and Si appear to be under-abundant, possibly due to depletion into dust grains, on whose surface the H_2 formation is taking place. It is important to note that this abundance determination is based on a beam-smeared H I column density. If substantial sub-structure exists within the Effelsberg beam (~ 9 arcmin), as possibly implied by the existence of H_2 , the abundances cited above might be incorrect. Interestingly, the b -value for the atomic absorption is rather high ($\geq 20 \text{ km s}^{-1}$), indicating that the H_2 indeed resides only in the inner-most region of IV 19, surrounded by a much larger envelope (with a higher velocity dispersion) in which the bulk of the neutral gas is situated.

No H_2 absorption is seen in the Complex C component at -155 km s^{-1} , giving further observational evidence that this metal-poor HVC is not able to form and maintain diffuse molecular hydrogen (see Richter et al. 2001c). We estimate an upper limit of $\log N \leq 14.45$ (3σ) for the total H_2 column density in Complex C toward PG 1351+640. This limit is consistent with previous H_2 measurements in Complex C (Murphy et al. 2000; Richter et al. 2001c; Collins, Shull, & Giroux 2002).

4. Distribution of H_2 in IVCs

Only a few cases of H_2 absorption in IVCs have been reported in the literature (Gringel et al. 2000; Richter et al. 2001a, 2001b; Bluhm et al. 2001), and thus very little is known about the overall extent of molecular gas in intermediate-velocity clouds. Previous detections include the IV Arch, the LLIV Arch, and the IVC in front of the LMC. Column densities and molecular gas fractions derived from these studies are lower than those found in the IV Arch towards PG 1351+640, with logarithmic column densities between 14.1 to 15.7 and molecular hydrogen fractions, $\log f$, between -5.4 and -2.2 . All H_2 measurements so far imply a diffuse molecular gas phase in IVCs.

To learn more about the distribution of diffuse molecular hydrogen in IVCs and the physical conditions of the gas in which the H_2 resides, we have searched for H_2 absorption with FUSE in intermediate-velocity clouds towards ~ 200 extragalactic background sources, such as quasars and active galactic nuclei (AGNs), as well as two distant halo stars. This data is available from the survey of O VI absorption in the thick disk of the Milky Way, as described by Savage et al. (2002) and Wakker et al. (2002). It is important to note that this data set is inhomogeneous with respect to sky-coverage, signal-to-noise (S/N), and overall data quality. Most of the background sources are located in the northern Galactic sky, giving access to the large northern IVC complexes, such as the IV Arch and the LLIV Arch. As described in §2, only a small fraction of the suitable background sources observed with FUSE can actually be used to study interstellar absorption in IVCs due to the flux limitations of these objects. From the available sight lines, 56 have FUSE data with a S/N sufficient to study interstellar H_2 absorption, and are known to pass intermediate-velocity H I halo gas at $|b| > 25$, $|v_{LSR}| \geq 25 \text{ km s}^{-1}$, and $\log N(\text{H I}) \geq 19.0$. 44 of these are located in the northern Galactic sky, 12 in the south.

Table 2 lists the 56 background sources and their coordinates together with the IVC velocities and IVC H I column densities. IVC identifications have been adopted from Wakker (2001). H I 21cm emission line data for these directions is available from the Leiden-Dwingeloo Survey (Hartmann & Burton 1997), the Effelsberg 100m tele-

scope (Wakker et al. 2001), the Green Bank 140 ft telescope (Murphy et al. 1996), and the Villa Elisa observatory (Arnal et al. 2000). ⁷ For more details on the H I spectra see Wakker et al. (2001). Note that there are some sight-lines that have multiple IVCs in the direction of the background source. Here, we consider only multiple IVCs that can be resolved with FUSE (i.e., components that are separated in velocity by more than $20-25 \text{ km s}^{-1}$). Two sightlines (PKS 0558-504 and NGC 1705; formally included in Table 2) show H I 21cm IVC emission in three components that have no counterparts in any atomic absorption line in the FUSE spectrum; these emission features are probably caused by H I beam smearing effects and/or radio base-line calibration errors. We do not consider these cases any further. In summary, the FUSE data set consists of 61 convincingly detected H I IVC components at $\log N(\text{H I}) \geq 19.0$ that are also detected in FUV metal-line absorption. We consider H_2 absorption in these IVC components in the following paragraphs.

A S/N of ~ 9 (per resolution element) is typically required to identify IVC H_2 absorption in individual lines at equivalent widths of $\geq 50 \text{ m}\text{\AA}$. Generally, a clear identification is easier, if the IVC component is well separated from the local Galactic gas (i.e., at velocities $\geq 50 \text{ km s}^{-1}$). For one case (Mrk 9; see Table 2), the local Galactic H_2 absorption is so strong, that it totally overlaps possible $J = 0, 1$ H_2 absorption at intermediate velocities, so little can be said about IVC H_2 absorption in this particular case. Together with the varying strength of local Galactic H_2 absorption and the resulting difficulty of separating intermediate-velocity components at varying S/N from the local Galactic component, the detection limits for H_2 absorption at intermediate velocities vary typically between 20 and 80 $\text{m}\text{\AA}$. Note that the S/N and the 3σ detection limit may vary considerably within a spectrum due to flux variations and instrumental effects (e.g., fixed-pattern noise, blending problems, varying exposure times for different detector segments). Out of 29 IVC components in FUSE spectra that have relatively good S/N (typically ~ 9 and higher) and a sufficiently resolved IVC component, H_2 ab-

⁷The 3σ detection limits for $N(\text{H I})$ from these surveys typically vary between 3 and $10 \times 10^{18} \text{ cm}^{-2}$.

sorption in individual lines at intermediate velocities is clearly detected in 14 cases, including the sight lines to PG 0804+761 (sampling the LLIV Arch) and PG 1259+593 (sampling the IV Arch) for which IVC H_2 absorption was reported earlier in individual sight-line analyses (Richter et al. 2001a; 2001c). H_2 absorption in the IV Arch has also been reported for the line of sight toward HD 93521, using ORFEUS data (Gringel et al. 2000); this sight-line has been included in Table 2. We here do not consider H_2 absorption that has been detected in the low column density IVC gas ($\log N(H_1) < 19.0$) toward the LMC (Bluhm et al. 2001). This general direction will be studied in detail in a different paper (Richter, Sembach & Howk 2002). H_2 equivalent widths for the 10 previously unpublished IVC components are given in Table 3. We list six equivalent widths per IVC component, representing the most pronounced IVC H_2 features for each case. The number of H_2 IVC features detected typically varies between 10 and 20 per component and are mostly $3 - 5\sigma$ detections. In Table 4 we list H_2 column densities, $\log N(J)$ and $\log N(H_2)_{\text{total}}$, and b -values that emerge from a fit of the data points in a fashion similar to that described for PG 1351+640 (see §3 and Figure 6). With the exception of NGC 4151, the 1σ uncertainties for the total H_2 column densities (see last column of Table 4) are higher than for PG 1351+640. The main contribution to the error is the determination of b , which turns out to be problematic for many of the IVC H_2 components where the S/N is low and/or the number of H_2 lines for certain values of J is limited due to blending problems. More accurate data are required to improve the accuracy of the determinations of $\log N(H_2)$. In all 14 cases, the fraction of hydrogen in molecular form is small ($\log f < -3$).

For the sight line towards 3C 273, Sembach et al. (2001b) have reported H_2 absorption in FUSE data at positive velocities around $+16 \text{ km s}^{-1}$, offset from the main local Galactic absorption (near -15 km s^{-1} , see their paper for details). The H_1 21cm emission line data from the Greenbank 140ft telescope (Murphy et al. 1996) is quite complex and shows three main H_1 components: a narrow emission feature near -6 km s^{-1} and two broad components located near -20 km s^{-1} and $+25 \text{ km s}^{-1}$. We have re-analyzed the FUSE data of

3C 273 using the newest available version of the FUSE pipeline (v2.0.5) in order to clarify the H_2 velocity structure of the individual Galactic absorption components. The new reduction (which provides a significantly improved velocity calibration of the FUSE data) confirms that the main H_2 absorption is offset in velocity from the main local absorber near -15 km s^{-1} . It is now clear that the H_2 absorption is related to the H_1 IVC gas at positive velocities around $+25 \text{ km s}^{-1}$. We therefore have included the line of sight towards 3C 273 as a positive detection of H_2 at IVC velocities in our sample (see Table 2). The H_2 column density listed in Table 2 has been adopted from Sembach et al. (2001b), since (except for the velocity calibration) the shape of the H_2 absorption spectrum produced by the v2.0.5 pipeline is identical with the spectrum from the earlier pipeline version used by Sembach et al. (2001b).

Figure 8 shows typical H_2 absorption profiles for the cases in which IVC H_2 absorption is newly detected (plots for PG 1259+593 are presented in Richter et al. 2001c). The IVC components and the local Galactic component are marked for each profile with dotted lines. Total H_2 column densities are also listed in Table 2, together with the molecular hydrogen fractions, $\log f$, based on the H_1 column densities from the 21cm observations listed in the seventh column of Table 2.

For the remaining IVC components in FUSE data with low S/N we find evidence for H_2 absorption in IVC gas in additional 17 cases. We have produced co-added composite velocity profiles for each spectrum including several H_2 lines from various transitions in order to improve the S/N and to study the general velocity extent of the H_2 absorption. We claim a tentative detection of H_2 in IVC gas (labeled as “possible” detections in Table 2), when the composite H_2 absorption profile shows $\geq 3\sigma$ evidence for an absorption component at intermediate velocities that would match the H_1 21cm emission line data. However, more accurate data are required to confirm the presence of IVC H_2 for these cases. 3σ upper limits for the total H_2 column densities and the molecular hydrogen fractions are listed in Table 2. The column density limits are based on the 3σ equivalent width limits of various blend-free H_2 transitions from the rotational states $J = 0 - 4$ that have been measured for each of the 17 IVC components. The total

H_2 column density limit for each IVC component has been calculated using a curve-of-growth technique, assuming that $b \geq 3 \text{ km s}^{-1}$ for all $N(J)$. Figure 9 shows three examples of co-added composite H_2 velocity profiles for NGC 7714, Mrk 357, and Mrk 618. At least three H_2 lines have been co-added together per sight line, suggesting that H_2 absorption is possibly present at IVC velocities along each sight line.

We find no evidence for H_2 absorption at IVC velocities in 30 of the 61 IVC components measured with FUSE. Upper limits for the H_2 column densities and the molecular hydrogen fractions (derived using the same procedure as for the tentative cases) are given in Table 2. It is possible, however, that diffuse molecular hydrogen is present below the detection limit. This is particularly likely for spectra that have low S/N (see last column of Table 2). A good example for this is the FUSE spectrum of PG 1259+593: H_2 in the IV Arch is detected at a very low column density of $\log N = 14.10$ at a very high S/N of ~ 30 . If the S/N were lower by 50 percent, H_2 in the IV Arch would be totally invisible along this sight line. Therefore, it is likely that with a better overall data quality the fraction of sight lines showing H_2 in IVC gas would increase substantially. For the IVC component at $+62 \text{ km s}^{-1}$ towards NGC 3783, Sembach et al. (2001a) give an upper limit for the H_2 column density of $\log N(H_2) \leq 15.00$, assuming that $b \geq 5 \text{ km s}^{-1}$. Using our method as described above we allow b -values as low as 3 km s^{-1} , so we find for the same component a more conservative upper limit of $\log N(H_2) \leq 15.84$ for the same FUSE data. For the second IVC component along this sight line at $+34 \text{ km s}^{-1}$ (see Table 2), we find an even higher limit of $\log N(H_2) \leq 16.52$ due to the fact that this component is partly blended by the local Galactic absorption near zero velocities.

Summarizing, we have investigated molecular hydrogen absorption with FUSE in 61 H_1 IVC components. Significant H_2 absorption is detected and measured in 14 cases. An additional 17 components show evidence for H_2 absorption, but more precise data is required to confirm the presence of H_2 . No evidence for H_2 is seen for 30 IVC components, but H_2 might be present at levels below the individual detection limits.

5. Comparison with H_1 Observations

Figure 10 shows the location of the 56 IVC sight lines (as listed in Table 2) in the northern and southern Galactic sky in polar projection, plotted over the IVC H_1 21cm distribution at intermediate velocities between $v_{\text{LSR}} = -30$ to -90 km s^{-1} (from data of the Leiden-Dwingeloo survey, Hartmann & Burton 1997).

Filled boxes show the directions, in which H_2 is detected at IVC velocities, filled triangles mark the low-S/N cases where IVC H_2 is possibly detected, and open circles indicate the non-detections. IVC H_2 absorption has a distribution as widespread as that of the H_1 21cm emission, although there are some sight lines, where H_1 emission is seen at $\log N \geq 19.3$ but no H_2 absorption is detected, even at high S/N (e.g., Mrk 209).

In Figure 11 we have plotted the fraction of hydrogen in molecular form, $\log f = \log [2N(H_2)/(N(H_1) + 2N(H_2))]$ against the logarithmic H_1 column density (from the 21cm data) for the 61 IVC components listed in Table 2. In this plot, the H_2 detections are plotted as filled circles, whereas the possible detections and the non-detections have open symbols (open triangles for the possible detections, open circles for the non-detections). Note that all open symbols plotted in Figure 11 therefore represent upper limits for $\log f$, while the filled circles show measured molecular hydrogen fractions. The very inhomogeneous data quality of the sample clearly hampers a statistical analysis of the H_2 fraction in IVCs as a function of the total gas column density. Data points for $\log f$ vary between -1.4 (upper limit) and -5.3 (measured value); thus they span a range over ~ 4 orders of magnitude. For the positive H_2 detections there is no visible correlation between $\log f$ and $\log N(H_1)$ and the scatter for the data points in $\log f$ is substantial. One could expect a correlation in the way that the molecular hydrogen fraction increases with the total gas column along the sight line because of H_2 line self-shielding. The fact that no correlation is seen implies that the H_2 absorption comes from low-column density H_2 absorbers without self shielding, while the scatter could be due to the varying number of H_2 absorbers per sight line. However, the observed scatter may also indicate that a) the H_1 column densities measured in 21cm do not represent accu-

rate values for the pencil beam sight lines because of beam-smearing effects, b) some fraction of the neutral gas is not physically related to the molecular material along the various lines of sight.

It is interesting that all of the detected H₂ IVC components have low molecular hydrogen fractions with $\log f \leq -3.3$. This suggests that for the many upper limits with $\log f > -3.3$ there is a substantial number of IVC components that have molecular material at H₂ fractions that are undetectable at the current S/N of the FUSE data. From the 29 data points with $\log f \leq -3.0$ there are 14 positive detections, 4 possible detections, and 11 non-detections. If this distribution is representative, H₂ at low molecular fractions may exist in over 50 percent of all IVC components that have H I column densities $\log N(\text{H I}) \geq 19.00$ and thus is a surprisingly widespread constituent of the gas in the lower Galactic halo. For the 14 positive IVC H₂ detections the mean logarithmic molecular hydrogen fraction is -4.3 .

6. Origin of the H₂

To understand the presence of molecular hydrogen in IVCs and its role for the interstellar gas in the lower Milky Way halo it is important to consider possible formation sites of the H₂.

Although it may be possible that molecular cloud complexes are pushed out of the disk of the Milky Way by energetic events (see Leass et al. 2002, in preparation), it appears very unlikely (and there is no observational evidence) that entire molecular clouds are transported several kiloparsecs above the Milky Way disk, and that the observed H₂ represents a diffuse remnant from dense molecular clouds that have been elevated from the disk into the halo. Two noticeable exceptions may be the Draco cloud and IV 21 (see above), which have been detected in CO emission, but these IVCs are located in the disk-halo interface ($z \leq 500$ pc) and they may well be “normal” molecular clouds at exceptionally large z -heights. Also, the presence of dust and heavy elements in halo clouds that contain H₂ implies that the observed molecular gas phase is not sampling any primordial molecular gas clumps in the halo that have been proposed in the literature as candidates for baryonic dark matter (e.g., de Paolis et al. 1995, Kalberla, Shchekinov & Dettmar

1999). The roughly solar abundances that are found in IVCs instead suggests that this gas represents Galactic disk material that is somehow circulating from the disk into the halo and back, possibly by way of a Galactic Fountain (Shapiro & Field 1976). In this model, gas ejected out of the disk by way of supernova explosions cools and falls back onto the Milky Way disk. Similar processes are probably also seen in other galaxies. For instance, the many extraplanar dust filaments observed in edge-on galaxies such as NGC 891 (Howk & Savage 1997) suggest that Fountain-type processes may be a rather common phenomenon in spiral galaxies.

The existence of diffuse H₂ at relatively low molecular hydrogen fractions implies that the H₂ line self shielding (see, e.g., Draine & Bertoldi 1996) is probably not very efficient in such gas. Without the self shielding, however, the photo-dissociation time scales are quite short ($\sim 10^3$ years), and no diffuse molecular material should be detectable, unless the dissociation is counteracted by local H₂ *formation*. Following this logic, the widespread existence of H₂ in IVCs strongly suggests that molecule formation takes place *in situ* in the most dense regions of IVCs. It has been proposed that halo clouds consist of a multi-phase structure (Wakker & Schwarz 1991; Wolfire et al. 1995) with cold, dense cores (“Cold Neutral Medium”, CNM) embedded in a more tenuous, warm medium (“Warm Neutral Medium”, WNM). Most likely, the diffuse molecular hydrogen forms in small, dense filaments during the cooling and fragmentation phase of a Galactic Fountain, and traces the CNM in the intermediate-velocity clouds. Houck & Bregman (1990) have developed a model for low-temperature Fountains with a cooling timescale, t_{cool} , of $\sim 3 \times 10^7$ yr, and a time scale for newly formed clouds to return to the disk, t_{ret} , on the order of 5×10^7 yr. This gives the CNM sufficient time to form H₂ at moderate densities to the fractional level that is observed (see §7.2). Since dust is available in IVCs, we assume that the H₂ formation takes place on the surfaces of dust grains, the most efficient way to form molecular hydrogen. One might argue that the grain formation rate in the halo must be significantly lower than in the disk due to the highly energetic processes operating that might destroy or at least modify the properties of the

dust grains. The results of Sembach & Savage (1996) in fact indicate that the surfaces of grains in halo clouds are probably different from those in diffuse disk clouds, but the implications for the halo H₂ grain formation rate are unclear. Franco et al. (1991) have presented the idea of a “soft” Galactic Fountain. They propose that dust grains might be transported into the halo due to radiation pressure of starlight near regions of intense star formation. It is shown that this “photolevitation” may push small diffuse clouds above the disk, whereas massive molecular clouds would not be affected by the momentum transfer from the radiation field. Such a process may only mildly modify the dust properties and could well explain the widespread presence of dust and molecular hydrogen in the lower Galactic halo. Franco et al. find that the photolevitation effect can maintain a neutral gas column density of $\sim 10^{20} \text{ cm}^{-2}$ above the disk, similar to what is found for most of the IVCs.

7. Physical Conditions

The overall ubiquity of H₂ in IVCs is indicating that these clouds must contain substructure, providing small, relatively dense clouplets and filaments that allow H₂ to form at a rapid enough rate to compensate for the destruction by UV photodissociation. In the following, we will investigate densities and typical dimensions of the structures in which the H₂ may reside by discussing the processes and parameters that balance the formation and dissociation of molecular hydrogen in Galactic halo clouds.

Since dust is present in IVCs (see Richter et al. 2001a, 2001b), we consider H₂ dust grain formation as the dominating H₂ formation process in IVCs and ignore any gas phase reactions (see Black 1978).

7.1. H₂ Formation-Dissociation Equilibrium

In an H₂ formation-dissociation equilibrium in transparent clouds, the H₂ volume density, $n(\text{H}_2)$, is related to the H I volume density, $n(\text{H I})$, via

$$\frac{n(\text{H I})}{n(\text{H}_2)} = \frac{\langle k \rangle \beta_0}{R n_{\text{H}}}, \quad (1)$$

where at low molecular hydrogen fractions $n_{\text{H}} =$

$n(\text{H I}) + 2n(\text{H}_2) \approx n(\text{H I})$ in cm^{-3} (Spitzer 1978, hereafter S78). In this equation, $\langle k \rangle \approx 0.11$ is the probability that the molecule is dissociated after photo absorption, β_0 is the photo-absorption rate per second, and R is the H₂ formation rate in units $\text{cm}^3 \text{s}^{-1}$.

The H₂ photo-absorption rate β_0 in the Galactic halo depends on the mean FUV radiation field at a height z above the Galactic plane. Principally, the FUV radiation field is expected to be lower in the Milky Way halo in comparison to the disk, and various attempts have been made to find scaling relations for the radiation field in the halo as function of the z -height (e.g., Wolfire et al. 1995). These studies show that only a fraction of the ultraviolet photons that are produced in the Galactic disk (mainly by OB stars) escape into the halo, mainly due to the extinction by dust grains. For the lower Galactic halo, the z -dependence of UV field in the halo is small due to the large solid angle of the Galactic plane. Using equation (4) from Wolfire et al. (1995), the FUV radiation field at a z -height of 1 kpc is reduced by a factor of ~ 2 in comparison to the midplane intensity. The H₂ photo-absorption rate in the halo is expected to scale directly with the halo UV field and thus is reduced by a similar factor. In the disk, the mean value for β_0 is $5.0 \times 10^{-10} \text{ s}^{-1}$ (S78). We therefore assume that $\beta_{0,\text{halo}} \approx 0.5 \beta_{0,\text{disk}} = 2.5 \times 10^{-10} \text{ s}^{-1}$ at the outer edge of an IVC. H₂ line self-shielding reduces the UV flux in the interior of a cloud once the H₂ column density in a single absorbing component exceeds a critical value. Following the approximation given by Draine & Bertoldi (1996), the H₂ photo-absorption rate then is reduced by the factor $S = (N(\text{H}_2)/10^{14} \text{ cm}^{-2})$ for H₂ column densities $\log N(\text{H}_2) \geq 14$. Whether or not the H₂ self-shielding is important for IVCs is unclear. The total H₂ column densities measured in IVCs are $\log N(\text{H}_2) = 14.1 - 16.4$, implying that for single-component absorbers self shielding may reduce the photo-absorption rate in the innermost region down to a level of $\sim 4.0 \times 10^{-12} \text{ s}^{-1}$. However, the relatively high b values measured for most of these clouds (Table 4) imply that there are several absorbing CNM structures within an IVC contributing to the total H₂ column density (see also discussion in §5), and H₂ self-shielding probably plays therefore only a minor role. We will discuss situations with and without self-shielding

at the end of this section.

Because we assume that all of the H_2 in IVCs forms on the surfaces of dust grains, the formation rate parameter R given in equation (1) denotes the rate per neutral H atom to form H_2 molecules by collisions with dust grains. R is a function of the gas and dust temperature, the sticking coefficient of H atoms on the grain surface, the mean projected surface area of the dust grains, and the mean H volume density (see S78). The value for R in Galactic halo clouds is unknown, as there is little knowledge about the properties of dust grains away from the Galactic disk. Here, we simply assume that $R_{\text{halo}} \approx R_{\text{disk}} = 3 \times 10^{-17} \text{ cm}^3 \text{ s}^{-1}$ (S78) due to the lack of better information. It is possible, however, that R_{halo} differs significantly from the value measured in the disk.

One major problem that arises from equation (1) is that the formation-dissociation equilibrium relates the volume densities n of H_1 and H_2 with each other, while column densities $N(H_1)$ and $N(H_2)$ are measured. It is often assumed that $N(H_1)/N(H_2) \approx n(H_1)/n(H_2)$ (see S78), but this assumption might be incorrect in the case of Galactic halo clouds because they likely have a pronounced multi-phase structure and unresolved sub-components. It is expected that IVCs (as well as HVCs) consist of large gaseous envelopes that contain both ionized and atomic species, interacting with the hot Galactic corona and residing in pressure equilibrium with the hot coronal gas (Spitzer 1956; Sembach et al. 2002). Most likely, the neutral and partly molecular cloud core that is associated with the CNM is embedded in a low density, higher temperature layer representing the WNM, but it is unknown in which phase the bulk of the gas is residing. In any case, the measured $N(H_1)$ represents the *total* column density of neutral hydrogen along the line of sight, and all gas phases that contain neutral gas at whatever fraction will contribute to its value. Thus, it appears not to be justified to simply compare $N(H_1)$ and $N(H_2)$ in IVCs, since the H_2 likely resides in regions much more confined than the H_1 , and only a fraction of the total H_1 is available for the formation of hydrogen molecules. The different gas phases (we here assume just two phases: neutral-molecular and neutral-ionized) should be treated separately, and a scaling factor for the H_1 column density in the IVCs is required. We define ϕ as an

H_1 scaling factor ≤ 1 , so that

$$\left(\frac{n(H_1)}{n(H_2)} \right)_f = \phi \frac{N(H_1)}{N(H_2)}, \quad (2)$$

where “f” stands for the dense filament in the CNM in which the H_2 gas resides, and $N(H_1)$ is the total H_1 column density of the IVC measured along the line of sight (*not* including other H_1 velocity components). Note that the molecular hydrogen fractions listed in Table 2 (tenth column) are derived in the standard way from the *total* IVC H_1 column densities given by the 21cm observations.

Using the values for β_0 and R for the Milky Way halo (as defined above) and equation (2), we find for the hydrogen volume density in the region of the IVC that contains the H_2 :

$$n_{H,f} \approx 9.2 \times 10^5 \frac{N(H_2)}{N(H_1)} \phi^{-1}. \quad (3)$$

Equation (3) allows us to determine the hydrogen volume density in the partly molecular cloud core of an IVC, assuming that the observed fraction of hydrogen in molecular form represents its abundance in formation-dissociation equilibrium.

If we neglect H_2 line self-shielding and take $N(H_2)/N(H_1) = 2.5 \times 10^{-5}$, $\beta_{0,\text{halo}} = 2.5 \times 10^{-10} \text{ s}^{-1}$, and $\phi = 0.5$ as typical values, we derive a hydrogen volume density of $n_{H,f} \approx 50 \text{ cm}^{-3}$ by using equation (3). If self-shielding is considered, the volume density is reduced by the factor S and could be as low as $\sim 1 \text{ cm}^{-3}$. However, if the CNM in IVCs is broken up into small column density filaments (see above), volume densities of $n_H = 10 - 50 \text{ cm}^{-3}$ appear to be more realistic.

For the somewhat stronger absorption in the IV Arch towards PG 1351+640 we have $N(H_2)/N(H_1) \approx 2.6 \times 10^{-4}$ (see §3), so that with $\phi = 0.5$ and without self-shielding the hydrogen volume density comes out as high as $n_{H,f} \approx 500 \text{ cm}^{-3}$. With self-shielding, we obtain $S = (2.69 \times 10^{16} \text{ cm}^{-2}/10^{14} \text{ cm}^{-2})^{-0.75} \approx 0.015$ and $n_{H,f} \approx 7 \text{ cm}^{-3}$. The actual value for $n_{H,f}$ probably lies somewhere in between, but without knowing the 3D structure of the H_2 absorber it is difficult to estimate a more realistic value for the self-shielding factor S . However, if we assume that the mean thermal pressure in the

CNM in these clouds is similar to that in the disk ($P_{\text{CNM}}/k = n_{\text{H}} T = 4000 \text{ cm}^{-3} \text{ K}$; Heiles 1997), the rotational excitation temperature $T_{01} = 141 \text{ K}$ derived in §3 implies $n_{\text{H,f}} \approx 30 \text{ cm}^{-3}$.

The linear thickness of such a CNM/H₂ structure, $D = \phi N(\text{H I})(n_{\text{H,f}})^{-1}$, is small, $\sim 0.1 \text{ pc}$ typically. Such a small filament is then probably surrounded by a low-density WNM envelope that has a much larger extent. Evidence for filamentary sub-structure of IVCs also comes from high-resolution optical spectra (Ryans, Sembach & Keenan 1996; Welty et al. 1999), in which multiple velocity components are detected in IVC gas separated only by a few km s^{-1} . Because of the close proximity of the components in velocity space it appears likely that they are physically related to each other (i.e., they are sub-components of the same IVC).

If IVCs are cooling and falling back onto the Milky Way disk (as indicated by their radial velocities), the most dense gas conglomerates may be located relatively close ($z < 1 \text{ kpc}$) to the midplane, i.e., in the disk-halo interface. At this stage, some of the molecular filaments might have turned dense enough to allow the formation of much larger amounts of H₂, and possibly carbon monoxide (CO). Interestingly, there are two IVCs known to exist in the disk-halo interface that are the *only* IVCs showing CO emission: the Draco cloud (Mebold et al. 1985) and IV 21 (Weiss et al. 1999; Heithausen et al. 2001). Possibly, these two clouds represent the final stage of a Galactic-Fountain IVC before re-entering the Milky Way disk.

7.2. H₂ Small-Scale Structure

We have shown at the end of the previous section the H₂ observations in IVCs suggest the presence of a large number of small, relatively dense filaments in the lower Milky Way halo, assuming that H₂ grain formation and photo-dissociation are equilibrated. In their best-fitting Galactic Fountain model (model 3), Houck & Bregman (1990) suggest a number of $\sim 9 \times 10^4$ halo clouds at a size of $\sim 2.7 \text{ pc}$ above a disk area of 1 kpc^2 . Assuming the thickness of typical H₂ filaments is only $\sim 0.1 \text{ pc}$, the relatively high detection rate of H₂ absorption measured in IVCs in this study implies that the number of H₂ bearing filaments per kpc^2 column is several orders of magnitude higher.

It is likely that the diffuse H₂ gas traces the CNM in these clouds, and that this CNM is surprisingly widespread, given the high detection rate of H₂. We do not know, however, whether these structures already represent the highest density regions in IVCs, or whether more dense molecular clumps with higher molecular fractions exist. H₂ absorption line measurements are naturally biased towards diffuse clouds with low molecular fractions and low densities due to their large volume filling factor. The chance to detect such a diffuse H₂ absorber by way of absorption spectroscopy towards a limited number of background sources is much higher than to find a small, dense clump that would have a small angular extent. It has been demonstrated over the last few years that the ISM consists of substantial small-scale structure at AU scales (e.g., Faison et al. 1998; Lauroesch, Meyer & Blades 2000), indicating apparently ubiquitous tiny gaseous structures (“tiny-scale atomic structures”, TSAS) with very high densities ($n_{\text{H}} \sim 10^3 - 10^5 \text{ cm}^{-3}$). The TSAS are probably filamentary and sheet like structures embedded in the CNM (Heiles 1997), but very little is known about their physical properties. Very recently, tiny-scale structure in the ISM has also been found in CO emission (Heithausen 2002), showing that molecules may play an important role for the understanding of these structures.

AU scale structure is also present in IVCs, as demonstrated by Na I observations of Complex gp against the globular cluster M 15 (Meyer & Lauroesch 1999). At such high volume densities, those tiny structures in the halo should contain molecular hydrogen at a high fractional abundance, since the dissociating FUV field in the halo is not intense and the H₂ formation time scale ($t_{\text{form}} = (R_{\text{halo}} n_{\text{H}})^{-1}$) becomes short at high densities. For $n_{\text{H}} = 300 \text{ cm}^{-3}$ the linear thickness would be 10 times smaller than for $n_{\text{H}} = 30 \text{ cm}^{-3}$, if the H I column density stays constant. However, the surface filling factor would be down by a factor of 100 (assuming spherical geometry). Thus, it would require a larger sample of FUSE sight lines to be able to detect and measure H₂ absorption in these smallest structures, and to investigate the relation between the TSAS and the more diffuse CNM phase in intermediate-velocity clouds. A possible candidate for molecular absorption related to TSAS could be the intermediate- and high-velocity

H_2 gas towards LH 58 in the Large Magellanic Cloud (Richter, Sembach & Howk 2002; Richter et al. 1999).

8. Discussion

Our study reveals that diffuse molecular hydrogen is a widespread, but not very abundant constituent in intermediate-velocity clouds in the low Galactic halo. The results suggest that the H_2 in IVCs resides in a large number of small, relatively dense filaments, associated with the CNM in these clouds.

The ubiquity of H_2 in IVCs underlines that molecular hydrogen is able to form and survive in regions that have low HI column densities, tracing the most dense regions in the diffuse interstellar medium. A key point for the formation and survival of H_2 in IVCs is that these clouds contain heavy elements and dust grains, on which H_2 formation proceeds very efficiently. Moreover, the FUV radiation field in IVCs is relatively low, reducing the UV photo-dissociation of H_2 . That the presence of dust and the absence of a strong UV field is so important for the existence of diffuse interstellar H_2 becomes immediately clear when comparing our findings with observations of H_2 in other environments. For the Magellanic Clouds, Richter (2000) and Tumlinson et al. (2002) find that the average molecular hydrogen fraction is significantly lower than in the Milky Way, mainly because of the very strong UV radiation from the many young OB stars in the Clouds, and due to the lower dust abundance. In the Magellanic Stream, Sembach et al. (2001a) and Richter et al. (2001c) find H_2 absorption in two of two available sight lines at column densities of $\log N(\text{H}_2) = 16 - 17$. The Magellanic Stream contains heavy elements and dust (Lu et al. 1998), thus allowing H_2 grain formation. In addition, the UV radiation field in the Magellanic Stream is expected to be low, resulting in a rather moderate H_2 photo-dissociation rate (see Sembach et al. 2001a). However, a low UV radiation field alone is not sufficient to allow diffuse H_2 to exist at moderate densities, as demonstrated by the many non-detections of H_2 in metal-poor, intergalactic $\text{Ly}\alpha$ clouds (e.g., Petitjean, Srianand & Ledoux 2000), and in high-velocity cloud Complex C. Towards PG 1259+593, Richter et al. (2001c) have studied H_2 absorption

in Complex C at a relatively high HI column density of $\log N(\text{H}\text{I}) \approx 20$. No H_2 was found down to a level of $\log N(\text{H}_2) \approx 14$, although newer Westerbork HI 21cm interferometer data clearly shows, that this sight line passes a very confined HI clump. Complex C is more than 6 kpc away from the Galactic plane and thus the UV radiation field in Complex C is expected to be at least as low as in IVCs. A detailed heavy element abundance study (Richter et al. 2001b) shows that Complex C has a ~ 0.1 solar metallicity in this direction and the abundance pattern implies that there is no or only very little dust present. Therefore, H_2 grain formation is suppressed, and gas phase formation processes (Black 1978) are obviously not efficient enough to allow diffuse H_2 gas to exist in Complex C, even at relatively high HI column densities.

The current H_2 absorption line data strongly suggest that the interplay of dust abundance and UV radiation field is of prime importance for the abundance of diffuse molecular hydrogen in the low-redshift Universe. Still, many of the H_2 formation/destruction aspects remain unknown, such as the grain-formation rates in environments with low metallicities and precise UV photo-dissociation rates. As we have shown, IVCs in the Milky Way halo represent an interesting case for the study of H_2 in diffuse solar-metallicity gas that is exposed to a moderate UV radiation field. Its widespread distribution shows that H_2 might be a rather robust constituent of the diffuse ISM, if the overall conditions are appropriate. High S/N FUSE observations are desirable to derive precise H_2 column densities, molecular fractions, excitation temperatures in Galactic halo clouds, and to search for the presence of high-density H_2 clumps in IVCs and HVCs. Such measurements might be of great importance for understanding and predicting the abundance of diffuse H_2 in the more distant Universe, where H_2 is very difficult to measure systematically with absorption spectroscopy.

9. Summary

We have used FUSE absorption line data to study the molecular hydrogen (H_2) content of intermediate-velocity clouds (IVCs) in the lower halo of the Milky Way.

(1) From 61 H_I IVC components that are sampled in a FUSE data set of 56 sight lines at latitudes $|b| > 25$, $|v_{\text{LSR}}| \geq 25 \text{ km s}^{-1}$, and $\log N(\text{H}_\text{I}) \geq 19.0$, we have detected and analyzed molecular hydrogen absorption in 14 cases in FUSE data with sufficient S/N (~ 9 per resolution element, and higher). For an additional 17 IVC components with lower S/N we also find evidence for IVC H₂ absorption, but cannot claim a firm detection. Thirty IVC components show no evidence for the presence of H₂.

(2) We have measured H₂ column densities, $\log N(\text{H}_2)$, and molecular hydrogen fractions, $\log f$, for the 14 positive IVC H₂ detections, and upper limits for $\log N(\text{H}_2)$ and $\log f$ for the remaining 47 components. For the positive IVC H₂ detections, $\log f$ varies between -3.3 and -5.3 , with a mean of -4.3 , implying a mostly atomic gas phase. Only 29 IVC components are sampled with FUSE data at a sufficient S/N to measure $\log f$ in the range ≤ -3.0 (14 detections, 4 possible detections, and 11 non-detections). For the rest of the data, IVC H₂ might also be present at low molecular fractions, but cannot be detected at the current data quality. Our study reveals that intermediate-velocity clouds in the halo of the Milky Way contain a ubiquitous, diffuse molecular hydrogen component.

(3) We have performed a detailed analysis of H₂ absorption in the Intermediate-Velocity Arch (core IV 19) in the direction of the quasar PG 1351+640. This sight line has the most pronounced case of H₂ absorption in IVCs found so far. We find a total H₂ column density of $\log N = 16.43 \pm 0.14$, and a molecular hydrogen fraction, $\log f$, of -3.3 . The low b -values ($b = 2.3 - 3.5 \text{ km s}^{-1}$) suggest that the IVC H₂ gas resides in a very confined clump in this direction. Two excitation temperatures are required to describe the rotational excitation of the H₂ gas: for $J = 0$ and 1 we derive $T_{01} = 141 \pm 20 \text{ K}$, possibly representing an upper limit for the kinetic temperature of the gas. For $J = 2 - 4$ we find $T_{24} = 885 \pm 270 \text{ K}$.

(4) We have discussed the physical conditions in IVCs that are required to describe the distribution and properties of the observed H₂. The solar metallicities of IVCs, as well as their radial ve-

locities, imply that most of these clouds represent the return flow of a Galactic Fountain, and that the H₂ is forming on the surface of dust grains in the halo during the cooling and fragmentation process. If the H₂ stays in formation-dissociation equilibrium, the molecular material must reside in a large number of small ($D \sim 0.1 \text{ pc}$), rather dense ($n_\text{H} \sim 30 \text{ cm}^{-3}$) filaments. Most likely, the H₂ gas traces the Cold Neutral Medium in these clouds. We speculate that more dense regions with higher molecular fractions could exist, associated with Tiny Scale Atomic Structures. These would be difficult to be detected in H₂ absorption due to their small size.

(5) H₂ measurements in intermediate- and high-velocity clouds, in local Galactic gas, in the Magellanic Clouds, and in intergalactic Ly α absorbers indicate that the interplay between dust and the UV radiation field is crucial for the abundance and distribution of diffuse H₂ in the low-redshift Universe. If dust is present and the FUV radiation field is moderate, H₂ appears to be a widespread constituent of the diffuse interstellar medium.

This work is based on data obtained for the the Guaranteed Time Team by the NASA-CNES-CSA FUSE mission operated by the Johns Hopkins University. Financial support has been provided by NASA contract NAS5-32985. PR is supported by the *Deutsche Forschungsgemeinschaft*. We thank the referee for helpful comments.

REFERENCES

Abgrall, H. & Roueff, E. 1989, A&AS, 79, 313
 Anders, E. & Grevesse, N. 1989, Geochim. Cosmochim. Acta 53, 197
 Arnal, E.M., Bajaja, E., Larrarte, J.J., Morras, R., Pöppel, W.G.L. 2000, A&AS, 142, 35
 Black, J. 1978, ApJ, 222, 125
 Bluhm, H., de Boer, K., Marggraf, O., Richter, P. 2001, A&A, 367, 299
 Browning, M.K., Tumlinson, J., Shull, J.M. 2002, ApJ, in press
 Collins, J.A., Shull, J.M., & Giroux, M.L. 2002, ApJ, in press

de Paolis, F., Ingrosso, G., Jetzer, P., Qadir, A., Roncadelli, M. 1995, *A&A*, 299, 647

Draine, B.T. & Bertoldi F. 1996, *ApJ*, 468, 269

Faison, M.D., Goss, W.M., Diamond, P.J., Taylor, G.B. 1998, *AJ*, 116, 2916

Franco, J., Ferrini, F., Ferrara, A., Barsella, B. 1991, *ApJ*, 366, 443

Gibson, B.K., Giroux, M.L., Penton, S.V., Putman, M.E., Stocke, J.T., Shull, M.J. 2000, *AJ*, 120, 1830

Gibson, B.K., Penton, S.V., Giroux, M.L., Stocke, J.T., Shull, M.J., Putman, M.E. 2001, *AJ*, 122, 3280

Grevesse, N. & Noels, A. 1993, in *Origin of the Elements*, ed. N. Prantzos, E. Vangioni-Flam, & M. Cassé, (Cambridge: Univ. Press), 15

Gringel, W., Barnstedt, J., de Boer, K.S., Grewing, M., Kappelmann, N., Richter, P. 2000, *A&A*, 358, L37

Hartmann, D. & Burton, W.B. 1997, *Atlas of Galactic Neutral Hydrogen*, Cambridge University Press

Heiles, C. 1997, *ApJ*, 481, 193

Heithausen, A., Weiss, A., Kerp, J., Fritz, T. 2001, *ApJ*, 561, 238

Heithausen, A. 2002, *A&A*, in press (astro-ph 0208531)

Houck, J.C. & Bregman, J.N. 1990, *ApJ*, 352, 506

Howk, J.C. & Savage, B.D. 1997, *AJ*, 114, 2463

Kalberla, P.M.W., Shchekinov, Y.A. & Dettmar, R.J. 1999, *A&A*, 350, L9

Kulkarni, S.R. & Fich, M. 1985, *ApJ*, 289, 792

Kuntz, K.D. & Danly, L. 1996, *ApJ*, 457, 703

Lauroesch, J.T., Meyer, D.M. & Blades, J.C. 2000, *ApJ*, 543, L43

Lehner, N., Sembach, K.R., Lambert, D.L., Ryans, R.S.L., Keenan, F.P. 1999, *A&A*, 352, 257

Lu, L., Sargent, W.L.W., Savage, B.D., Wakker, B.P., Sembach, K.R., Oosterloo, T.A. 1998, *AJ*, 115, 162

Mebold, U., Cernicharo, J., Velden, L., Reif, K., Crezelius, C., Goerigk, W. 1985, *A&A*, 151, 427

Meyer, D.M. & Lauroesch, J.T. 1999, *ApJ*, 520, L103

Moos, H.W., et al. 2000, *ApJ*, 538, L1

Murphy, E.M., Lockman, F.J., Laor, A., Elvis, M. 1996, *ApJS*, 105, 369

Murphy, E.M., et al. 2000, *ApJ*, 538, L35

Petitjean, P., Srianand, R. & Ledoux C. 2000, *A&A*, 364, L26

Richter, P., de Boer, K.S., Widmann, H., Kappelmann, N., Gringel, W., Grewing, M., Barnstedt, J. 1999, *Nature*, 402, 386

Richter, P. 2000, *A&A*, 359, 111

Richter, P., Savage, B.D., Wakker, B.P., Sembach, K.R., Kalberla, P.M.W. 2001a, *ApJ*, 549, 281

Richter, P., et al. 2001b, *ApJ*, 559, 318

Richter, P., Sembach, K.R., Wakker, B.P., Savage, B.D. 2001c, *ApJ*, 562, L181

Richter, P., Sembach K.R. & Howk J.C. 2002, *A&A*, submitted

Ryans, R.S.I., Sembach, K.R. & Keenan, F.P. 1996, *A&A*, 314, 609

Sahnow, D.J., et al. 2000, *ApJ*, 538, L7

Savage, B.D., et al. 2002, *ApJ*, submitted

Sembach, K.R. & Savage, B.D. 1996, *ApJ*, 457, 211

Sembach, K.R., Howk, J.C., Savage, B.D., Shull, J.M. 2001a, *AJ*, 121, 992

Sembach, K.R., Howk, J.C., Savage, B.D., Shull, J.M., Oegerele, W.R 2001b, *ApJ*, 561, 573

Sembach, K.R., et al. 2002, *ApJ*, submitted

Shapiro, P.R., & Field, G.B. 1976, *ApJ*, 205, 762

Shull, J.M. & Beckwith, S. 1982, *ARA&A*, 20, 163

Spitzer, L. 1956, ApJ, 124, 20

Spitzer, L. (S78), ‘Physical Processes in the Interstellar Medium’, 1978, Wileys Classics Library, ISBN 0-471-02232-2

Tumlinson, J., et al. 2001, ApJ, 566, 857

Turner, J., Kirby-Docken, K., Dalgarno, A. 1977, ApJS, 35, 281

Wakker, B.P. & Schwarz, U.J. 1991, A&A, 250, 484

Wakker, B.P., et al. 1999, Nature, 402, 388

Wakker, B.P. 2001, ApJS, 136, 463

Wakker, B.P., Kalberla, P.M.W., van Woerden, H., de Boer, K.S., Putman M.E. 2001, ApJS, 136, 537

Wakker, B.P., et al. 2002, ApJS, submitted

Weiss, A., Heithausen, A., Herbstmeier, U., Mebold, U. 1999, A&A, 344, 955

Welty, D.E., Frisch, P.C., Sonneborn, G., York, D.G. 1999, ApJ, 512, 636

Wolfire, M.G., McKee, C.F., Hollenbach, D., Tielens, A.G.G.M. 1995, ApJ, 453, 673

Fig. 1. $\text{H}\alpha$ 21cm IVC sky (Aitoff projection) from the Leiden-Dwingeloo sky survey (LDS; Hartmann & Burton 1997) for LSR velocities between -30 and -90 km s^{-1} and $\text{H}\alpha$ column densities between 2 and $70 \times 10^{19} \text{ cm}^{-2}$, plotted in Galactic coordinates (l, b) and centered on $l = 120$. The contours represent column densities of 2 and $10 \times 10^{19} \text{ cm}^{-2}$. For the identifications of the individual IVC complexes see Wakker (2001). Note that the LDS data does not fully cover the sky for $b \leq +30$ in the ranges $0 \leq l \leq +15$ and $230 \leq l \leq 360$ (see Hartmann & Burton 1997 for details).

Fig. 2. Continuum-normalized atomic absorption profiles of the FUSE spectrum of PG 1351+640 are plotted on a LSR radial velocity scale, and compared to $\text{H}\alpha$ 21cm emission line data from the Effelsberg 100m radio-telescope (see Wakker et al. 2001). Three major components are present at $v_{\text{LSR}} \approx 0, -50$ and -155 km s^{-1} , representing gas from the local Milky Way, the IV Arch (core IV 19, strongest component), and high-velocity cloud Complex C, respectively. Complex C absorption is present in the $\text{Si II } \lambda 1020.7$ and $\text{Fe II } \lambda 1122.0$ lines, but not in $\text{P II } \lambda 1152.8$. The $\text{H}\alpha$ emission line data contains substructure in each of the three components, such as another IVC component at -74 km s^{-1} (core IV 9), which is also present in the atomic absorption profiles.

Fig. 3. A portion of the FUSE spectrum of PG 1351+640 in the wavelength range between 1076.5 and 1079.5 \AA , sampling the H_2 2 – 0 Lyman band. The individual H_2 lines present in the data are labeled above the spectrum. The data plotted here shows H_2 absorption from rotational levels $J = 0, 1$ and 2 in two components at 0 and -50 km s^{-1} , representing H_2 gas in the local Milky Way disk and the IV Arch (IV 19), respectively. The solid gray line shows a two-component Gaussian fit of the spectrum that reproduces the absorption pattern seen in the FUSE data.

Fig. 4. Continuum-normalized H_2 absorption profiles in the FUSE spectrum of PG 1351+640 for the rotational levels $J = 0$ and 1 are plotted.

H_2 absorption is present in the local Milky Way component at zero velocities and in the IV Arch (IV 19) component at -50 km s^{-1} . H_2 lines are labeled in the upper left corner of each box (with ‘L’ for the Lyman band and ‘W’ for the Werner band). Lines from other transitions or species are marked with ‘b’.

Fig. 5. Same as Fig. 3, but for rotational levels $J = 2$ and 3 .

Fig. 6. Empirical curve of growth for H_2 absorption in the IV Arch (IV 19) toward PG 1351+640 for the rotational levels $J = 0 – 3$, as labeled in the lower right corner. Two very low b -values ($b = 2.3_{-0.5}^{+1.1} \text{ km s}^{-1}$ for $J = 0$ and $3.5_{-0.9}^{+1.4} \text{ km s}^{-1}$ for $J = 1 – 3$) are required to fit the data in the $\log(W_{\lambda}/\lambda) - \log(Nf\lambda)$ space, suggesting that the H_2 ground state absorption occurs in a very confined cloud core, whereas absorption from the excited levels arises from the surrounding gas that has a slightly higher velocity dispersion. A typical error bar that represents the 1σ uncertainty in the H_2 equivalent widths (see also Table 1) is shown in the lower left corner.

Fig. 7. H_2 rotational excitation in the IV Arch (IV 19) toward PG 1351+640. The logarithmic column densities of each rotational state, N_J , divided by the quantum mechanical statistical weight for each state, g_J , are plotted against the excitation energy, E_J . The dashed lines represent fits from a theoretical Boltzmann distribution. The rotational ground states, $J = 0$ and 1 , fit on a line that is equivalent to a Boltzmann temperature of $T_{01} = 141 \pm 20 \text{ K}$, possibly representing an upper limit for the kinetic temperature of the gas. The excited rotational levels, $J = 2, 3$ and 4 , fit on a line with $T_{24} = 885 \pm 270 \text{ K}$, possibly indicating processes like UV pumping, H_2 formation pumping, and shock excitation.

Fig. 8. FUSE continuum-normalized H_2 absorption profiles toward 9 background sources are shown. For each sight line, an H_2 absorption profile from the Lyman band (labeled in the lower

right corner) is plotted and compared to the H_I 21cm emission (labeled in the upper right corner) from either Green Bank data (GB), Effelsberg data (EB), or Leiden-Dwingeloo data (LD; see Wakker et al. 2001; Murphy et al. 1996; Hartmann & Burton 1997). The two major absorption components along each sight line from local Galactic gas near zero velocities and from halo gas at intermediate velocities between $25 \leq |v_{\text{LSR}}| \leq 100 \text{ km s}^{-1}$ are marked with dashed lines. IVC H₂ absorption that matches the H_I 21cm emission line data is present in each of the absorption profiles. Stellar background sources are labeled with a star symbol behind the object name. Lines from other transitions or species are marked with ‘b’. The abbreviation ‘N.F.’ is used for the normalized flux.

Fig. 9. Composite H₂ absorption profiles for NGC 7714, Mrk 357, and Mrk 618, representing examples of tentative H₂ detections at IVC velocities in FUSE data with low S/N. At least three H₂ lines per sight line have been stacked on top of each other in order to study the velocity extent of H₂ in these directions. As in the previous figure, H_I 21cm data is plotted above each H₂ absorption profile. The local Galactic components and the IVC components are marked with dashed lines. In the three examples shown, H₂ appears to be present at IVC velocities, but more accurate absorption line data are required to confirm these detections.

Fig. 10. North- and south-polar sky distribution of the 56 sight lines that sample H_I IVC gas for $|b| \geq 25$ and $25 \leq |v_{\text{LSR}}| \leq 100 \text{ km s}^{-1}$, plotted on top of the H_I 21cm IVC sky from the Leiden-Dwingeloo Survey (Hartmann & Burton 1997; H_I data plotted for $-30 \leq v_{\text{LSR}} \leq -90 \text{ km s}^{-1}$; see also Fig. 1 for details). Definitive IVC H₂ detections are marked with filled boxes, while tentative detections are labeled with filled triangles; non-detections are marked with open circles (see also Table 2). The H₂ absorption generally follows the H_I emission for regions with high H_I column densities. Note that the H_I data show IVC gas solely at negative radial velocities, while for some lines of sight that are labeled here the

main IVC component is at *positive* velocities (see Table 2). The position of the Magellanic Clouds (LMC+SMC) is also indicated.

Fig. 11. The logarithmic H₂ fraction, $\log f = \log [2N(\text{H}_2)/(N(\text{H}_I) + 2N(\text{H}_2))]$, is plotted against the logarithmic H_I 21cm column density, $\log N(\text{H}_I)$, for the 61 IVC components listed in Table 2. H₂ detections are plotted as filled circles, possible detections and the non-detections have open symbols (open triangles for the possible detections, open circles for the non-detections; note that these symbols represent upper limits for $\log f$). All IVC components in which H₂ is clearly detected (14 components) have $\log f \leq -3$.

TABLE 1
 H_2 EQUIVALENT WIDTHS^a FOR THE IV ARCH TOWARDS PG 1351+640

Line	λ_{vac} ^b [Å]	$\log \lambda f$ ^b	$W_{\lambda \text{ IVC}}$ [mÅ]
$J = 0; \log N(0) = 15.80 \pm 0.21$			
R(0),8-0	1001.828	1.432	37 ± 12
R(0),0-0 ^{c,d}	1008.559	1.647	98 ± 23
R(0),6-0	1024.376	1.473	54 ± 11
R(0),4-0	1049.367	1.383	35 ± 9
R(0),2-0	1077.142	1.111	32 ± 9
R(0),1-0	1092.200	0.802	33 ± 7
R(0),0-0	1108.130	0.275	28 ± 13
$J = 1; \log N(1) = 16.23 \pm 0.14$			
P(1),8-0	1003.302	0.948	57 ± 9
R(1),5-0	1037.150	1.271	83 ± 12
R(1),4-0	1049.960	1.225	53 ± 20
P(1),4-0	1051.033	0.902	50 ± 9
P(1),3-0	1064.606	0.805	47 ± 11
R(1),2-0	1077.702	0.919	51 ± 9
P(1),2-0	1078.929	0.624	54 ± 11
R(1),1-0	1092.737	0.618	49 ± 8
P(1),1-0	1094.057	0.340	57 ± 9
R(1),0-0	1108.636	0.086	48 ± 9
$J = 2; \log N(2) = 14.91 \pm 0.33$			
R(2),8-0	1003.989	1.232	≤ 30
P(2),8-0	1005.398	0.998	≤ 27
R(2),0-0 ^c	1009.023	1.208	33 ± 9
Q(2),0-0 ^c	1010.938	1.385	43 ± 12
R(2),7-0 ^e	1014.980	1.285	30 ± 10
P(2),7-0	1016.466	1.007	36 ± 8
R(2),4-0	1051.498	1.168	29 ± 11
P(2),4-0	1053.284	0.982	≤ 68
R(2),3-0	1064.994	1.069	38 ± 9
P(2),1-0	1096.444	0.420	≤ 57
$J = 3; \log N(3) = 15.33 \pm 0.26$			
P(3),7-0	1019.507	1.050	42 ± 10
P(3),6-0	1031.195	1.055	54 ± 9
P(3),5-0	1043.504	1.060	56 ± 10
R(3),4-0	1053.975	1.137	≤ 58
P(3),4-0	1056.471	1.006	47 ± 9
R(3),3-0	1067.478	1.066	41 ± 6
P(3),3-0	1070.141	0.910	≤ 35
P(3),1-0	1099.792	0.439	29 ± 11
$J = 4; \log N(4) \leq 14.64$			
P(4),6-0	1035.184	1.056	≤ 33

TABLE 1—*Continued*

Line	$\lambda_{\text{vac}}^{\text{a}}$ ^b [Å]	$\log \lambda f^{\text{b}}$	$W_{\lambda \text{ IVC}}$ [mÅ]
R(4),5-0	1044.543	1.195	≤ 44
R(4),3-0	1070.899	1.012	≤ 27
$\log N(\text{Total}) = 16.43 \pm 0.14$			

^aEquivalent widths and 1σ errors (or 3σ upper limits) are listed for the -50 km s^{-1} IVC absorption.

^bVacuum wavelengths and oscillator strengths from Abgrall & Roueff (1989).

^cLine from the Werner band.

^dBlended together with Werner Q(1),0-0 & Lyman P(3),8-0.

^eBlended together with Werner Q(4),0-0.

TABLE 2
FUSE SURVEY OF H₂ IN INTERMEDIATE-VELOCITY CLOUDS

Object	Type	<i>l</i>	<i>b</i>	<i>v</i> _{IVC} ^a [km s ⁻¹]	IVC Name	log <i>N</i> (H ₁) _{IVC}	IVC H ₂ Status	log <i>N</i> (H ₂) _{IVC}	log <i>f</i> ^f _{IVC}	Remarks
Mrk 509	QSO	35.97	-29.86	+60	Complex gp	19.51 ^b	yes	14.92	-4.3	...
vZ 1128	Star	42.50	+78.68	+29	...	19.31 ^d	no evidence	≤ 15.04	≤ -4.0	...
Mrk 1513	Seyfert	63.67	-29.07	-29	...	19.37 ^b	no evidence	≤ 16.43	≤ -2.6	...
Mrk 501	BLLac	63.60	+38.86	-38	...	19.17 ^c	no evidence	≤ 17.08	≤ -1.8	low S/N ^m
PG 1444+407	QSO	69.90	+62.72	-30	...	19.53 ^b	no evidence	≤ 17.38	≤ -1.9	low S/N
Mrk 487	Galaxy	87.84	+49.03	-85	IV Arch (IV 15)	19.16 ^b	no evidence	≤ 17.43	≤ -1.4	low S/N
NGC 7714	Seyfert	88.22	-55.56	-50	...	19.40 ^b	possibly	≤ 17.03	≤ -2.1	low S/N
Mrk 876	QSO	98.27	+40.38	-30	Draco	19.84 ^c	yes	15.57	-4.0	...
NGC 7673	Galaxy	99.25	-35.40	-53	PP Arch	19.25 ^b	no evidence	≤ 17.14	≤ -1.8	low S/N
Mrk 817	Seyfert	100.30	+53.48	-40	IV Arch	19.33 ^c	no evidence	≤ 14.95	≤ -4.1	...
NGC 5461	M 101-H II	101.89	+59.76	-51	IV Arch (IV 19)	19.49 ^d	no evidence	≤ 16.32	≤ -2.9	low S/N
Mrk 335	Seyfert	108.76	-41.42	-27	...	20.00 ^b	possibly	≤ 15.82	≤ -3.9	low S/N
Mrk 59	Galaxy	111.54	+82.12	-44	IV Arch	19.31 ^d	yes	14.72	-4.3	...
PG 1351+640	QSO	111.89	+52.02	-47	IV Arch (IV 19)	20.05 ^c	yes	16.43	-3.3	see §3
				-74	IV Arch (IV 9)	19.20 ^c	no evidence	≤ 15.18	≤ -3.7	...
HD 121800	Star	113.01	+49.76	-70	IV Arch	19.86 ^c	yes	14.29	≤ -5.3	...
Mrk 279	Seyfert	115.04	+46.86	-40	LLIV Arch	19.80 ^c	no evidence	≤ 14.85	≤ -4.6	...
				-76	IV Arch (IV 9)	19.42 ^c	no evidence	≤ 14.85	≤ -4.3	...
PG 1259+593	QSO	120.56	+58.05	-54	IV Arch	19.50 ^c	yes	14.10 ^g	≤ -5.1	...
PG 0052+251	QSO	123.91	-37.44	-39	...	19.82 ^b	possibly	≤ 17.12	≤ -2.4	low S/N
Mrk 352	Seyfert	125.03	-31.01	-28	...	20.33 ^b	possibly	≤ 17.05	≤ -3.0	low S/N
Mrk 205	Seyfert	125.45	+41.67	-48	LLIV Arch	19.71 ^b	possibly	≤ 16.69	≤ -2.7	low S/N
3C 249.1	QSO	130.39	+38.55	-50	LLIV Arch	19.80 ^b	possibly	≤ 17.00	≤ -2.5	low S/N
Mrk 357	Seyfert	132.20	-39.14	-41	...	19.58 ^d	possibly	≤ 17.16	≤ -2.1	low S/N
NGC 3516	Seyfert	133.24	+42.40	-47	LLIV Arch	19.91 ^b	possibly	≤ 17.23	≤ -2.4	low S/N
Mrk 209	Galaxy	134.15	+68.08	-55	IV Arch	19.61 ^b	no evidence	≤ 16.79	≤ -2.5	...
				-100	IV Arch (IV 4)	19.06 ^b	no evidence	≤ 16.79	≤ -2.0	...
PG 0804+761	QSO	138.28	+31.03	-58	LLIV Arch	19.56 ^c	yes	14.71 ^h	-4.5	...
NGC 3690	Galaxy	141.91	+55.41	-54	IV Arch	19.56 ^b	no evidence	≤ 16.77	≤ -2.5	...
HS 0624+6907	QSO	145.71	+23.35	-27	LLIV Arch	20.15 ^c	no evidence	≤ 17.41	≤ -2.4	low S/N
PG 0832+675	Star	147.75	+35.01	-50	LLIV Arch	19.99 ^c	yes	15.76	-3.9	...
NGC 4151	Seyfert	155.08	+75.06	-29	IV Arch (IV 26)	20.20 ^b	yes	15.36	-4.5	...
NGC 3310	Seyfert	156.60	+54.06	-47	IV Arch	19.80 ^b	yes	14.95	-4.5	...
Mrk 9	Seyfert	158.36	+28.75	-40	LLIV Arch	19.60 ^b	possibly	≤ 16.48	≤ -2.8	strong local H ₂
NGC 4214	Galaxy	160.24	+78.07	-33	IV Arch (IV 26)	20.13 ^d	possibly	≤ 15.74	≤ -4.1	...
Mrk 116	Galaxy	160.53	+44.84	-39	LLIV Arch	19.48 ^c	possibly	≤ 16.35	≤ -2.8	low S/N
Mrk 106	Seyfert	161.14	+42.88	-40	LLIV Arch	19.35 ^c	possibly	≤ 17.48	≤ -1.6	low S/N
NGC 1068	Seyfert	172.10	-51.93	-58	...	19.08 ^b	no evidence	≤ 15.26	≤ -3.5	...
PG 0953+414	QSO	179.79	+51.71	-49	IV Arch (IV 16)	19.33 ^c	no evidence	≤ 15.07	≤ -4.0	...
Mrk 421	BLLac	179.83	+65.03	-61	IV Arch (IV 26)	19.78 ^b	no evidence	≤ 14.93	≤ -4.5	...
PG 0947+396	QSO	182.85	+50.75	-66	IV Arch (IV 16)	19.68 ^b	no evidence	≤ 17.11	≤ -2.3	low S/N
HD 93521	Star	183.14	+62.15	-62	IV Arch	19.58 ^e	yes	14.60 ⁱ	-4.7	ORFEUS
NGC 3991	Galaxy	185.68	+77.20	-53	IV Arch (IV 18)	19.86 ^e	no evidence	≤ 17.26	≤ -2.3	low S/N
Ton 1187	QSO	188.33	+55.38	-27	IV Arch	19.55 ^b	no evidence	≤ 17.40	≤ -1.9	low S/N
				-69	IV Arch	19.47 ^b	no evidence	≤ 17.40	≤ -1.8	low S/N
PG 1001+291	QSO	200.09	+53.20	-32	IV Arch (IV 18)	20.12 ^b	possibly	≤ 17.18	≤ -2.6	low S/N
HE 0238-1904	QSO	200.48	-63.63	-42	...	19.33 ^d	no evidence	≤ 17.10	≤ -1.9	low S/N
Mrk 36	Galaxy	201.76	+66.49	-55	IV Arch (IV 18)	19.83 ^d	possibly	≤ 17.15	≤ -2.4	low S/N

TABLE 2—Continued

Object	Type	<i>l</i>	<i>b</i>	$v_{\text{IVC}}^{\text{a}}$ [km s $^{-1}$]	IVC Name	$\log N(\text{H}_1)_{\text{IVC}}$	IVC H ₂ Status	$\log N(\text{H}_2)_{\text{IVC}}$	$\log f^{\text{f}}$ IVC	Remarks
NGC 3504	Galaxy	204.60	+66.04	-52	IV Arch (IV 18)	19.85 ^d	possibly	≤ 16.33	≤ -3.2	low S/N
Mrk 618	Seyfert	206.72	-34.66	-27	...	19.56 ^b	possibly	≤ 17.15	≤ -2.1	low S/N
PG 1116+215	QSO	223.36	+68.21	-42	IV Spur	19.83 ^c	yes	15.27	-4.3	...
Mrk 734	Seyfert	244.75	+63.94	-42	IV Spur	19.81 ^b	no evidence	≤ 16.90	≤ -2.6	low S/N
PKS 0558-504	QSO	257.96	-28.57	+26	...	20.31 ^e	[no evidence]	no atomic absorption seen
				+71	...	19.62 ^e	[no evidence]	no atomic absorption seen
HD 100340	Star	258.85	+61.23	-29	IV Spur	19.98 ^d	yes	15.98	-3.7	MWRS ^k
NGC 1705	Galaxy	261.08	-38.74	+87	...	19.64 ^e	[no evidence]	no atomic absorption seen
PG 1211+143	QSO	267.55	+74.32	-35	IV Spur	19.94 ^b	no evidence	≤ 15.23	≤ -4.4	...
Mrk 771	Seyfert	269.44	+81.74	-29	IV Spur	19.93 ^b	no evidence	≤ 16.78	≤ -2.8	low S/N
NGC 3783	Seyfert	287.46	+22.95	+34	...	19.44 ^b	possibly	≤ 16.52	≤ -2.6	...
				+62	...	20.00 ^b	no evidence	$\leq 15.84^{\text{k}}$	≤ -3.9	...
3C 273	QSO	289.95	+64.36	+25	...	19.42 ^b	yes	15.71 ^l	-3.4	...
HE 1228+0131	QSO	291.26	+63.66	+27	...	19.26 ^c	no evidence	≤ 15.96	≤ -3.0	low S/N
Tol 1247-232	Galaxy	302.60	+39.30	+54	...	19.40 ^d	no evidence	≤ 17.24	≤ -1.9	low S/N
ESO 141-G55	Seyfert	338.18	-26.71	-45	...	19.27 ^e	no evidence	≤ 17.02	≤ -2.0	...

^aLSR velocities, based on 21cm data, are listed; ^bH₁ 21cm data from the Greenbank 140ft telescope (Murphy et al. 1996); ^cH₁ 21cm data from the Effelsberg 100m telescope (Wakker et al. 2001); ^dH₁ 21cm data from the Leiden-Dwingeloo Survey (Hartmann & Burton 1997); ^eH₁ 21cm data from the Villa Elisa telescope (Arnal et al. 2000); ^f $\log f = \log [2N(\text{H}_2)/(N(\text{H}_1) + 2N(\text{H}_2))]$; ^gRichter et al. (2001c); ^hRichter et al. (2001a); ⁱGringel et al. (2000); ^jObserved through the medium-resolution aperture; ^kSee also Sembach et al. (2001a); ^lSee also Sembach et al. (2001b) and §4; ^mFUSE spectra with an average S/N < 9 (per resolution element); see also Wakker et al. (2002).

TABLE 3
SELECTED H₂ EQUIVALENT WIDTHS^a FOR IVCs

Line	λ_{vac} ^b [Å]	$\log \lambda f$ ^b	W_{λ} IVC [mÅ]
Mrk 509 - Complex gp			
R(0),0-0 ^{c,d}	1008.559	1.647	29 ± 5
R(1),4-0	1049.960	1.225	36 ± 6
R(2),7-0	1014.980	1.285	26 ± 8
R(3),6-0	1028.988	1.243	26 ± 4
R(3),4-0	1053.975	1.137	18 ± 5
P(3),4-0	1056.471	1.006	20 ± 4
Mrk 876 - Draco			
R(2),8-0	1003.989	1.232	26 ± 7
Q(2),0-0 ^c	1010.938	1.385	31 ± 6
R(2),3-0	1064.994	1.069	30 ± 6
R(3),0-0 ^c	1010.128	1.151	25 ± 5
P(3),5-0	1043.504	1.060	24 ± 6
R(3),4-0	1053.975	1.137	20 ± 5
Mrk 59 - IV Arch			
R(1),8-0	1002.457	1.256	35 ± 7
R(1),4-0	1049.960	1.225	38 ± 9
P(1),4-0	1051.033	0.902	20 ± 6
R(1),2-0	1077.702	0.919	23 ± 8
P(1),2-0	1078.929	0.624	21 ± 6
P(3),5-0	1043.504	1.060	23 ± 9
HD 121800 - IV Arch			
R(1),8-0	1002.457	1.256	14 ± 4
R(1),7-0	1013.441	1.307	17 ± 4
R(1),4-0	1049.960	1.225	25 ± 6
P(1),4-0	1051.033	0.902	12 ± 4
P(1),3-0	1064.606	0.805	18 ± 4
R(1),2-0	1077.702	0.919	11 ± 3
PG 1259+593 - IV Arch ^e			
R(1),8-0	1002.457	1.256	21 ± 5
Q(1),0-0 ^c	1009.770	1.384	19 ± 4
P(1),7-0	1014.332	0.960	13 ± 4
R(1),4-0	1049.960	1.225	14 ± 4
P(1),4-0	1051.033	0.902	10 ± 3
Q(2),0-0 ^c	1010.938	1.385	14 ± 4
PG 0832+675 - LLIV Arch			
P(2),6-0	1028.108	1.053	31 ± 9
R(2),5-0	1038.690	1.221	25 ± 7
R(2),4-0	1051.498	1.168	45 ± 12
P(3),5-0	1043.504	1.060	42 ± 7
R(3),4-0	1053.975	1.137	42 ± 8

TABLE 3—*Continued*

Line	$\lambda_{\text{vac}}^{\text{b}}$ [Å]	$\log \lambda f^{\text{b}}$	$W_{\lambda} \text{ IVC}$ [mÅ]
P(3),4-0	1056.471	1.006	30 ± 8
NGC 4151 - IV Arch (IV 26)			
P(1),5-0	1038.158	0.956	64 ± 12
P(1),4-0	1051.033	0.902	73 ± 16
P(3),6-0	1031.195	1.055	43 ± 5
R(3),5-0	1041.159	1.222	44 ± 5
P(3),5-0	1043.504	1.060	55 ± 8
R(4),5-0	1044.543	1.195	21 ± 7
NGC 3310 - IV Arch			
P(2),8-0	1005.398	0.998	33 ± 8
Q(2),0-0 ^c	1010.938	1.385	50 ± 9
P(2),4-0	1053.284	0.982	45 ± 9
R(3),7-0	1017.427	1.263	42 ± 8
R(3),4-0	1053.975	1.137	26 ± 6
P(3),4-0	1056.471	1.006	24 ± 5
PG 1116+215 - IV Spur			
R(0),4-0	1049.367	1.383	46 ± 5
R(0),2-0	1077.142	1.111	41 ± 5
R(1),4-0	1049.960	1.225	68 ± 8
R(1),2-0	1077.702	0.919	47 ± 6
P(1),2-0	1078.929	0.624	41 ± 9
Q(2),0-0 ^c	1010.938	1.385	38 ± 5
HD 100340 - IV Spur			
P(1),5-0	1038.158	0.956	74 ± 13
P(1),2-0	1078.929	0.624	64 ± 7
R(2),4-0	1051.498	1.168	20 ± 4
R(2),3-0	1064.994	1.069	27 ± 5
R(3),4-0	1053.975	1.137	17 ± 5
P(3),5-0	1043.504	1.060	9 ± 3

^aSix equivalent widths per sight line and 1σ errors (or 3σ upper limits) are listed.

^bVacuum wavelengths and oscillator strengths from Abgrall & Roueff (1989).

^cLine from the Werner band.

^dBlended together with Werner Q(1),0-0 & Lyman P(3),8-0.

^eSee also Richter et al. (2001c).

TABLE 4
NEWLY MEASURED H_2 COLUMN DENSITIES IN IVCs

Object	IVC Name	$\log N(0)$	$\log N(1)$	$\log N(2)$	$\log N(3)$	$\log N(4)$	b [km s^{-1}]	Total $\log N(H_2)$ ^b
Mrk 509	Complex gp	≤ 13.00	14.60	14.33	14.35	≤ 14.09	5.5	14.92 ± 0.46
Mrk 876	Draco	14.93	15.38	14.39	14.32	≤ 14.35	5.4	15.57 ± 0.23
Mrk 59	IV Arch	≤ 14.22	14.72	≤ 14.10	≤ 14.55	≤ 14.36	4.1	14.72 ± 0.28
HD 121800	IV Arch	≤ 13.94	14.29	≤ 14.27	≤ 14.23	≤ 14.19	3.0	14.29 ± 0.62
PG 1259+593	IV Arch	≤ 13.69	14.10	≤ 13.85	≤ 13.87	≤ 13.96	L^a	14.10 ± 0.19
PG 0832+675	LLIV Arch	15.47	15.25	14.57	14.80	≤ 14.30	5.3	15.76 ± 0.31
NGC 4151	IV Arch (IV 26)	14.86	14.98	14.39	14.58	≤ 14.14	L^a	15.36 ± 0.11
NGC 3310	IV Arch	≤ 16.50	≤ 16.11	14.76	14.49	≤ 14.35	7.4	14.95 ± 0.77
PG 1116+215	IV Spur	14.59	15.02	14.45	14.18	≤ 14.24	7.9	15.27 ± 0.34
HD 100340	IV Spur	15.66	15.67	14.34	13.99	≤ 13.85	6.6	15.98 ± 0.83

^aDerived column density assumes that the data points fall on the linear part of the curve of growth.

^b 1σ error is given.

Fig. 1.—

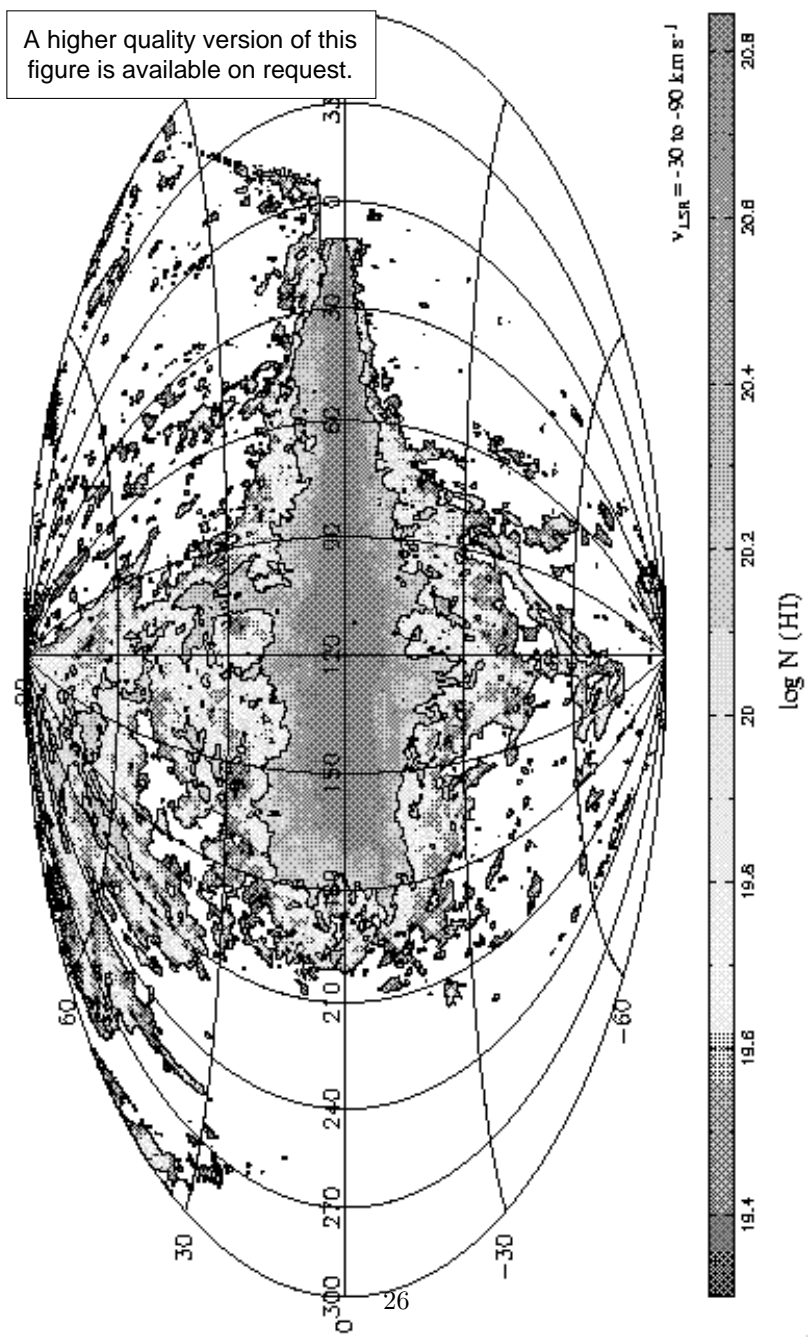


Fig. 2.—

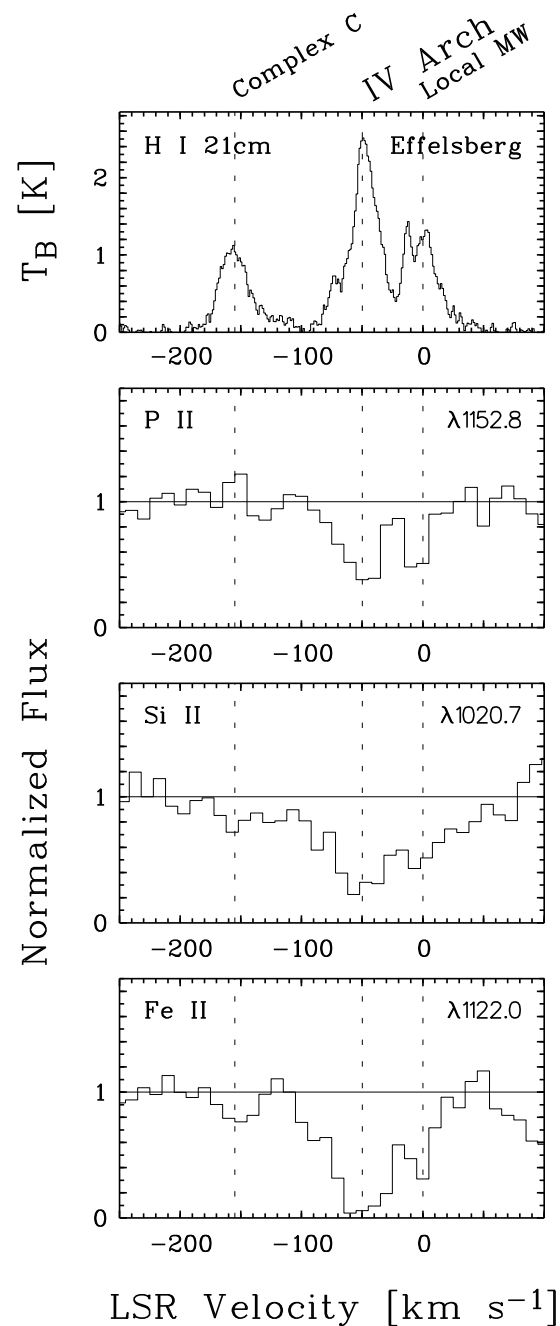


Fig. 3.—

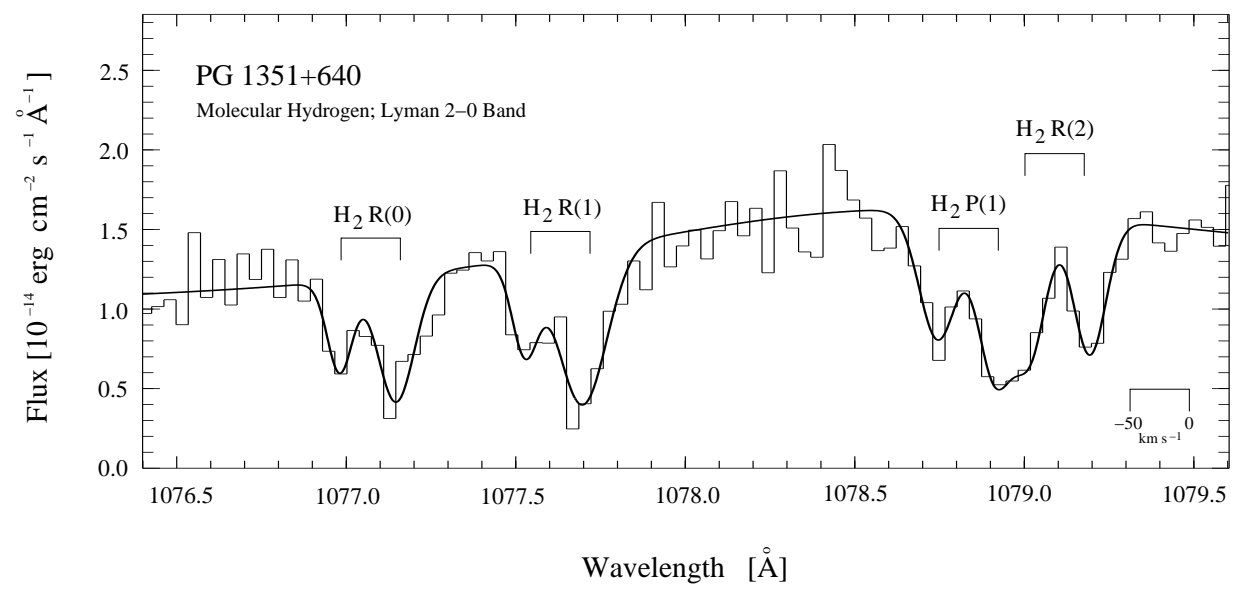


Fig. 4.—

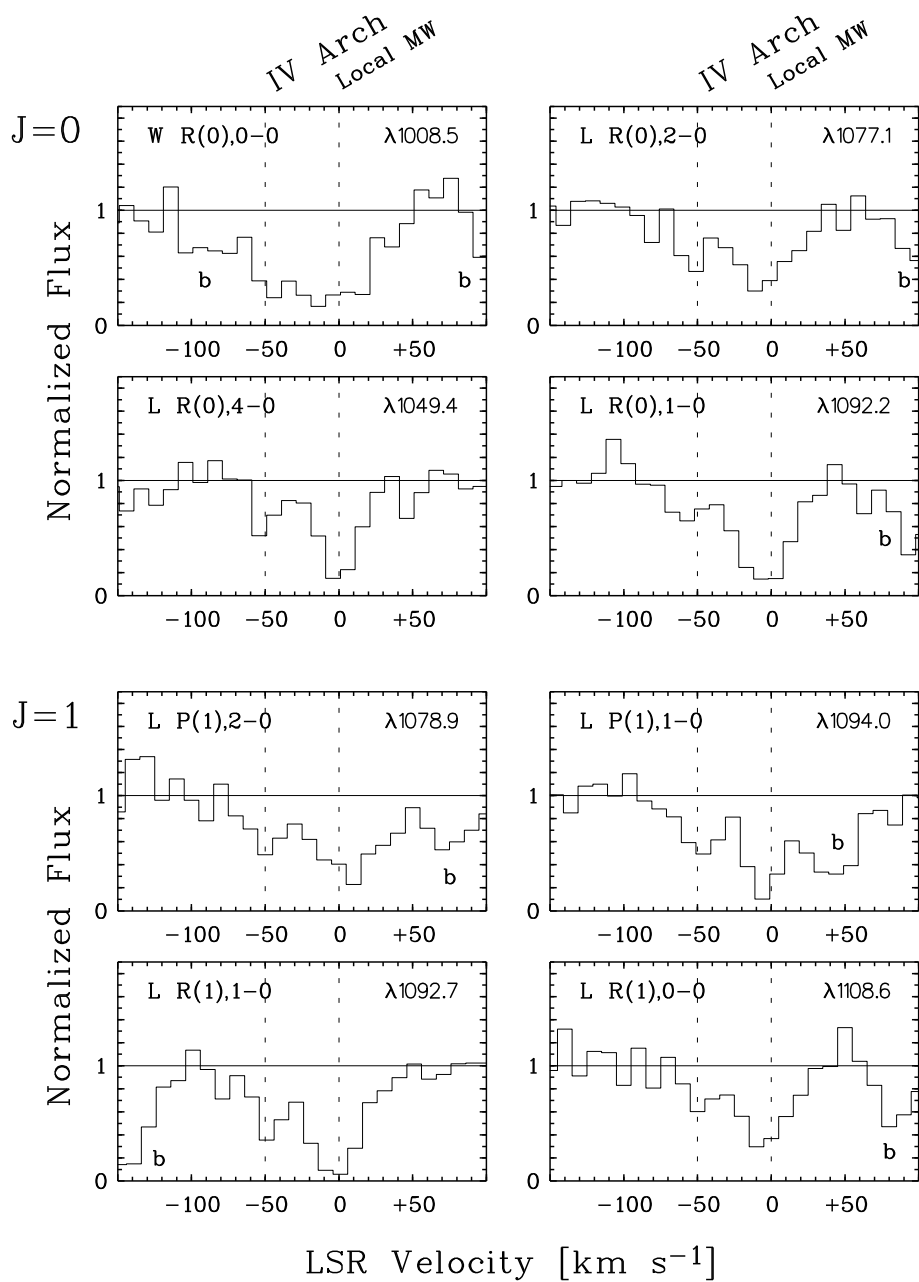


Fig. 5.—

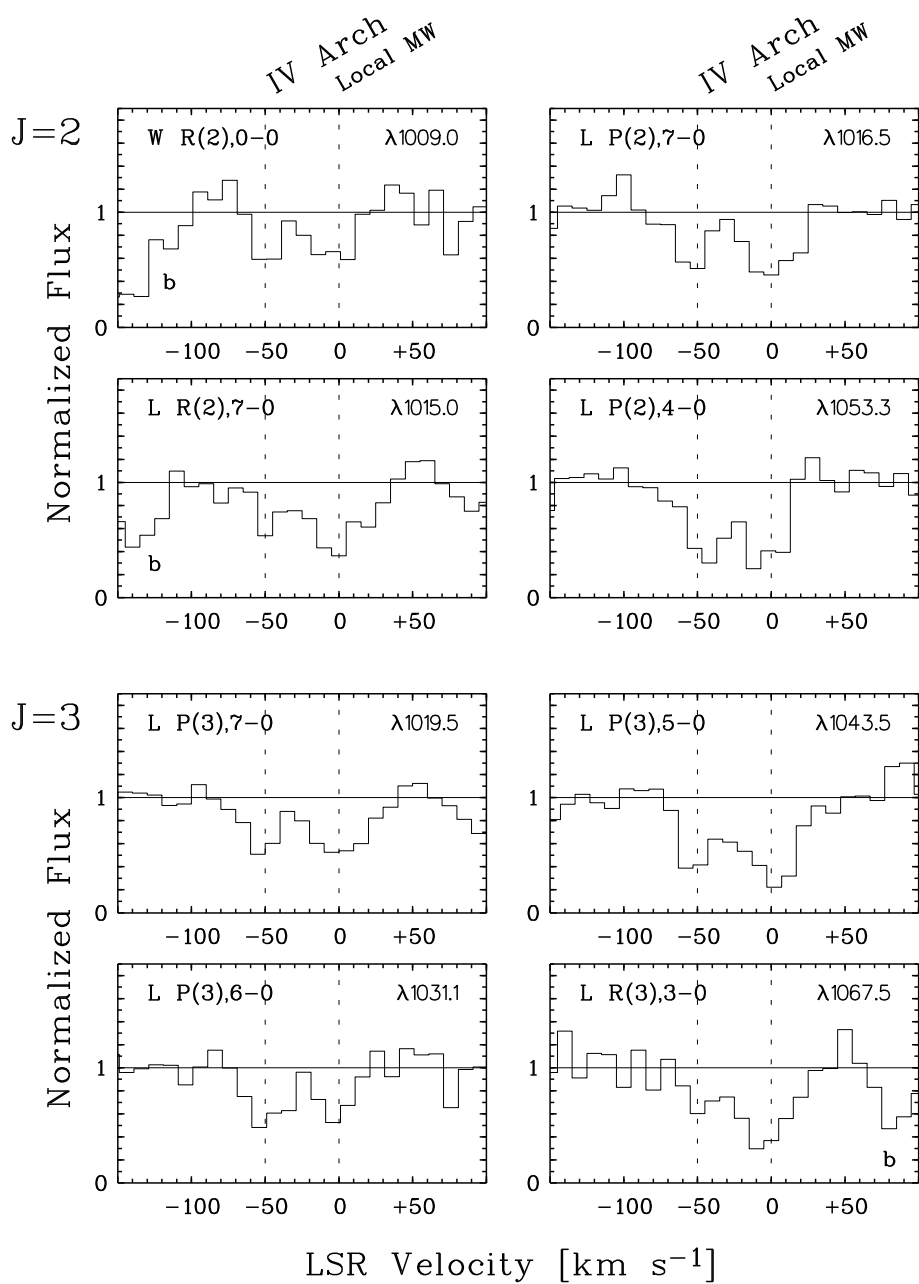


Fig. 6.—

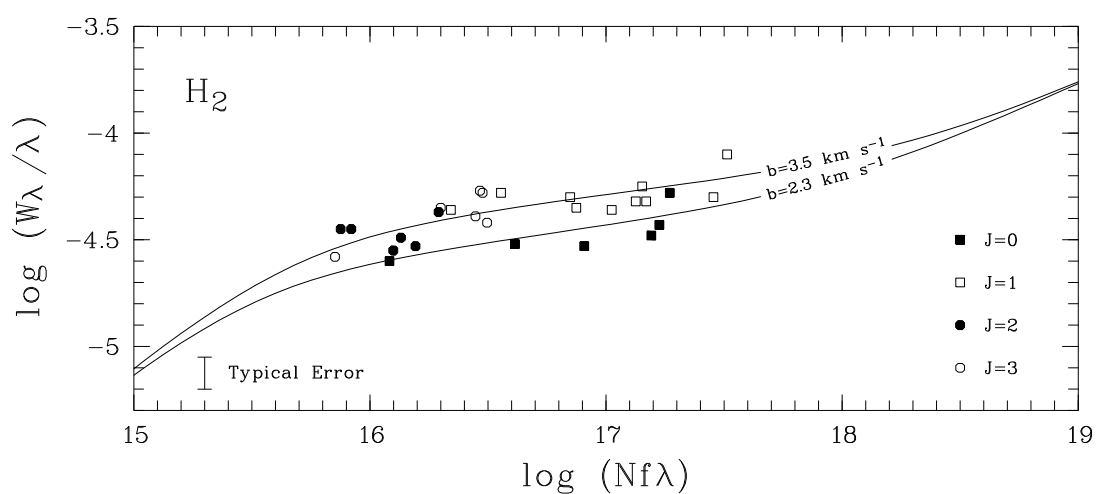


Fig. 7.—

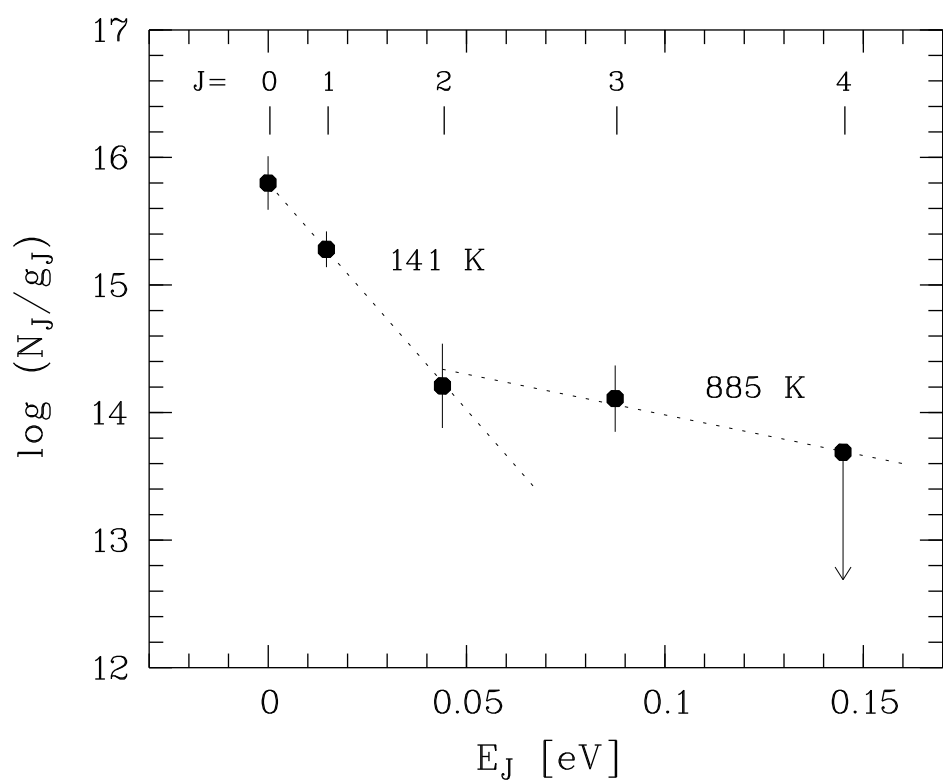


Fig. 8.—

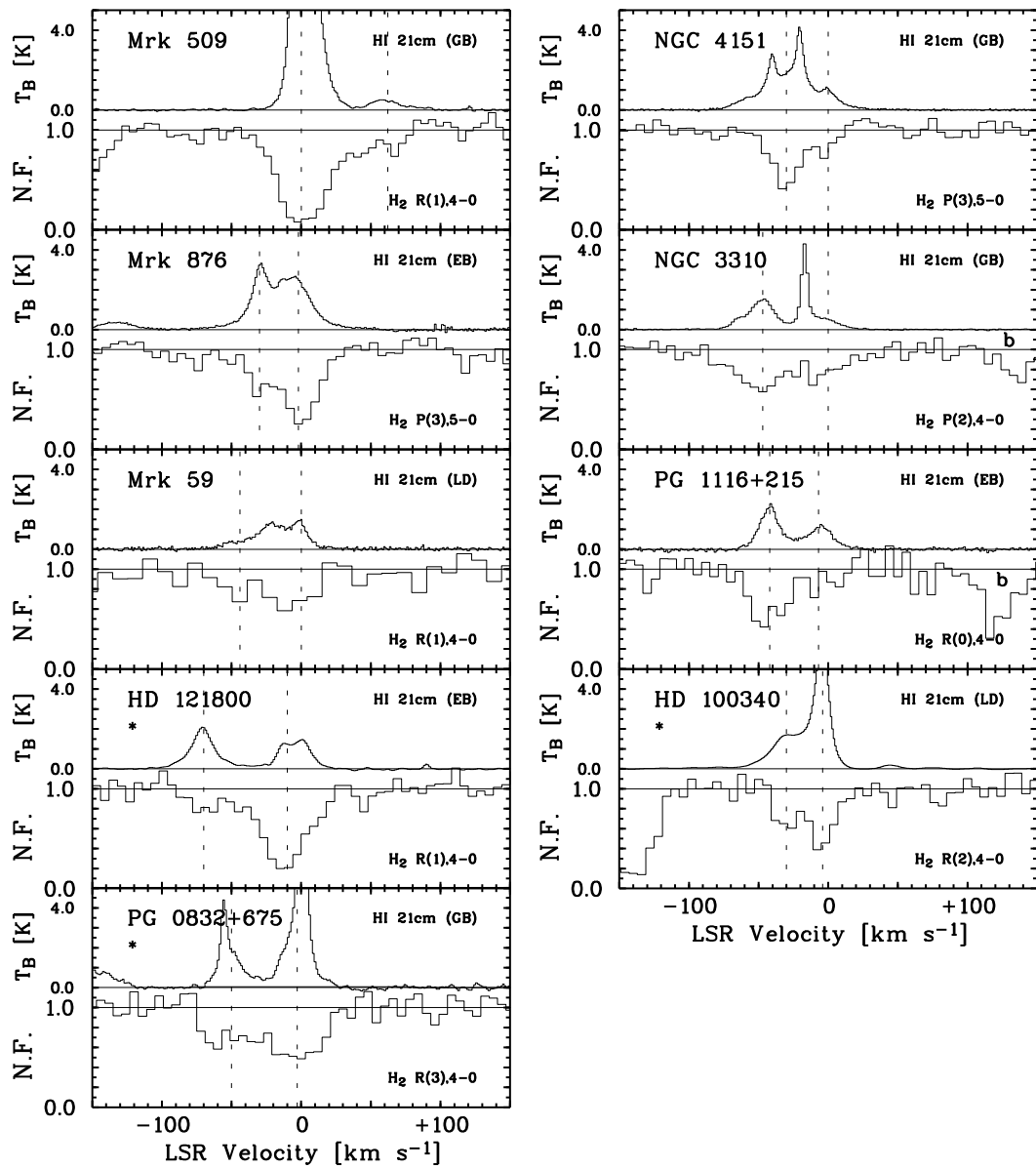


Fig. 9.—

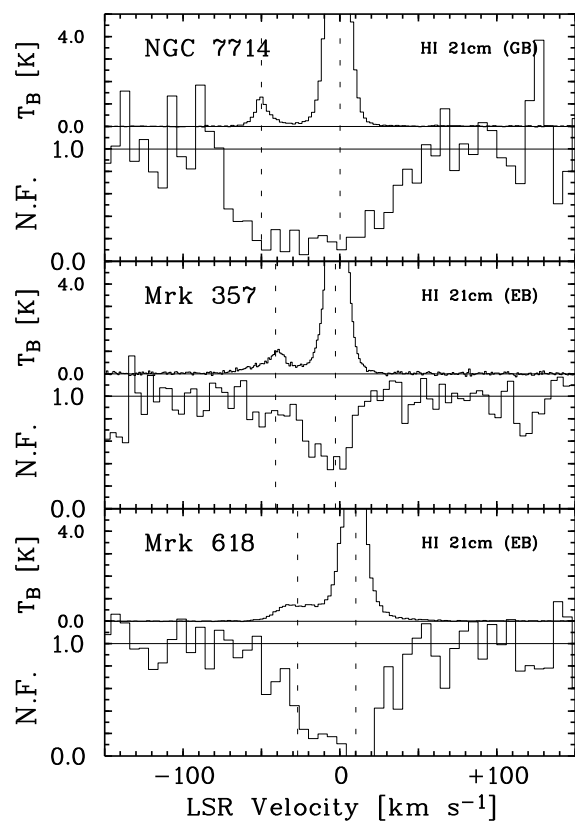


Fig. 10.—

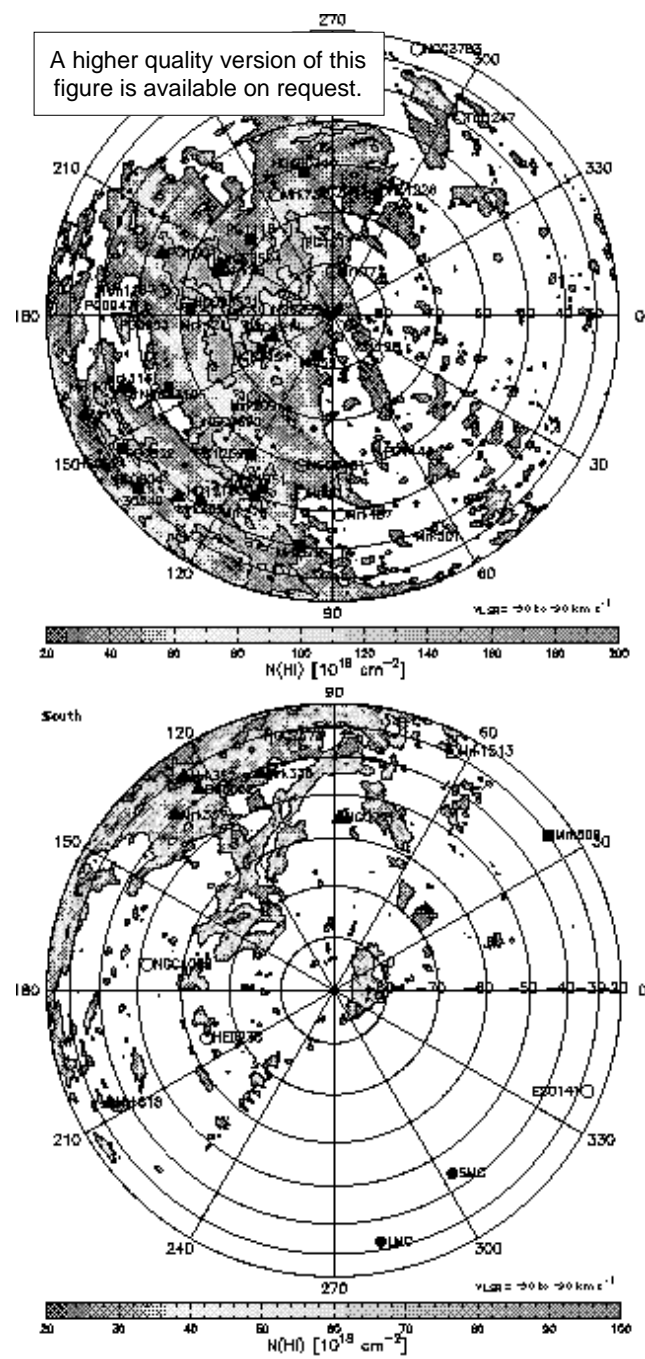


Fig. 11.—

